LASER & PHOTONICS REVIEWS

www.lpr-journal.org

Metal-nanoparticle plasmonics

Matthew Pelton[1], **Javier Aizpurua**[2], and **Garnett Bryant**[3]

[1] Center for Nanoscale Materials, Argonne National Laboratory, 9700 S. Cass Ave., Argonne, IL 60439, USA
[2] Donostia International Physics Center and Centro Mixto de Física de Materiales CSIC-UPV/EHU, Paseo Manuel Lardizabal 4, Donostia-San Sebastián 20018, Spain
[3] Atomic Physics Division and Joint Quantum Institute, National Institute of Standards and Technology, 100 Bureau Dr. MS 8423, Gaithersburg, MD 20899-8423, USA

Received 16 January 2008, revised 14 February 2008, accepted 18 February 2008
Published online 2 April 2008

Key words metal nanoparticles, nano-optics, optical properties, plasmonics, nonlinear optics
PACS 78.67.Bf, 73.20.Mf, 73.22.Lp, 78.47.-p, 81.16.Be, 81.16.Nd, 81.16.Dn

The rapid emergence of nanoplasmonics as a novel technology has been driven by recent progress in the fabrication, characterization, and understanding of metal-nanoparticle systems. In this review, we highlight some of the key advances in each of these areas. We emphasize the basic physical understanding and experimental techniques that will enable a new generation of applications in nano-optics.

2008

Laser & Photon. Rev. **2**, No. 3, 136 – 159 (2008) / **DOI** 10.1002/lpor.200810003

WILEY

REPRINT

Laser & Photon. Rev. **2**, No. 3, 136–159 (2008) / **DOI** 10.1002/lpor.200810003

Abstract The rapid emergence of nanoplasmonics as a novel technology has been driven by recent progress in the fabrication, characterization, and understanding of metal-nanoparticle systems. In this review, we highlight some of the key advances in each of these areas. We emphasize the basic physical understanding and experimental techniques that will enable a new generation of applications in nano-optics.

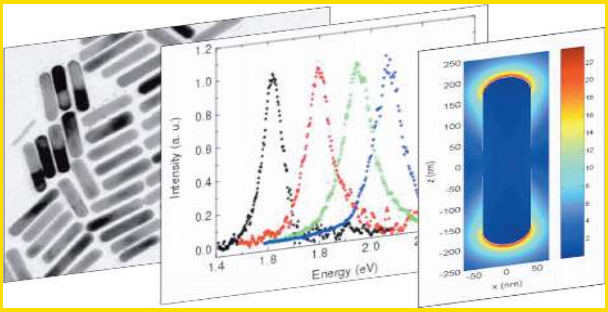

Critical areas driving the emergence of metal-nanoparticle plasmonics: fabrication, characterization, and theory.

© 2008 by WILEY-VCH Verlag GmbH & Co. KGaA, Weinheim

Metal-nanoparticle plasmonics

Matthew Pelton [1], *Javier Aizpurua* [2], *and Garnett Bryant* [3,*]

[1] Center for Nanoscale Materials, Argonne National Laboratory, 9700 S. Cass Ave., Argonne, IL 60439, USA
[2] Donostia International Physics Center and Centro Mixto de Física de Materiales CSIC-UPV/EHU, Paseo Manuel Lardizabal 4, Donostia-San Sebastián 20018, Spain
[3] Atomic Physics Division and Joint Quantum Institute, National Institute of Standards and Technology, 100 Bureau Dr. MS 8423, Gaithersburg, MD 20899-8423, USA

Received: 16 January 2008, Revised: 14 February 2008, Accepted: 18 February 2008
Published online: 02 April 2008

Key words: metal nanoparticles; nano-optics; optical properties; plasmonics; nonlinear optics

PACS: 73.20.Mf, 73.22.Lp, 78.47.-p, 78.67.Bf, 81.16.Be, 81.16.Dn, 81.16.Nd

1. Introduction

Metal nanoparticles (NPs) promise to play a central role in the emerging technological revolution that is pushing optics past the diffraction limit and fully into the nanometer size regime [1, 2]. The optical properties of noble metals such as gold and silver are governed primarily by coherent oscillations of conduction-band electrons, known as plasmons [3, 4]. The interaction between light and metal NPs, in particular, is dominated by localized surface plasmon resonances (LSPs), or charge-density oscillations on the closed surfaces of the particles [5, 6]. LSPs have the ability to strongly scatter and absorb light and to squeeze light into nanometer dimensions, producing large local enhancements of electromagnetic fields [7]. The science and technology that deals with the generation, control, manipulation, and transmission of these excitations in metal nanostructures has recently grown into an independent research field known as "plasmonics."

The extensive recent research effort in nano-plasmonics has largely been motivated by the potential for a strikingly diverse array of applications. To cite only a few examples, localized plasmons allow for biological spectroscopy in drastically reduced volumes [8–10], greatly increasing the signal strengths and resolution available in field-enhanced spectroscopies such as surface enhanced spectroscopy [11] and surface-enhanced infrared absorption [12]. Molecular fluorescence can be enhanced by attached NPs [13, 14], potentially enabling a new generation of light-emitting devices and novel forms of fluorescence microscopy. The ability of NPs to squeeze light into the nanoscale provides near-field optical microscopy with unprecedented resolution. [15–17] Arrays of metal NPs or structured metal films provide nanoscale control of the transmission, manipulation and switching of optical signals. [18–23] Advanced materials composed of metal nanostructures can have the novel optical properties, such as negative refraction [24–26], that are required to realize recent predictions of superlensing [27].

Corresponding author: e-mail: garnett.bryant@nist.gov

WILEY InterScience®
© 2008 by WILEY-VCH Verlag GmbH & Co. KGaA, Weinheim

Biomolecules labeled with metal NPs can be dynamically traced during biological processes [28, 29]. Moreover, functionalized NPs with appropriately tuned optical responses are being used for cancer diagnosis and therapy [30]. For example, metal NPs with resonances in the near infrared can be functionalized to selectively attach to tumor cells. Near-infrared bombardment of affected areas optically excites the NPs and thermally destroys the tumor cell. Metal NPs can also act as antennas in laser assisted remote release of encapsulated materials for drug delivery [31].

We can point to three main driving forces behind the recent development of NP plasmonics. First, the development of increasingly sophisticated lithographic and chemical methods now allow the routine production of a wide variety of complex NPs and their assemblies. The experimental capability to create metal NPs on demand together with the accessibility of techniques for versatile NP design have opened the possibility to synthesize and tune metal building blocks to control and engineer the plasmon response on the nanoscale. This control opens completely new possibilities in materials science, communications, biochemistry, and medicine.

Second, characterization methods have advanced greatly in the last decade by taking advantage of improved measurement technologies. While traditional ensemble measurements of optical absorption and scattering spectra continue to be crucial characterization tools, enhanced capabilities to monitor single particles, spatially map response on the nanoscale, and access ultrafast time scales have greatly extended the ability to probe NP plasmonics.

Finally, the modeling and simulation of the optical response of complex nanostructures have been greatly expanded, providing a detailed, quantitative understanding of these systems. These advances have stimulated a close interplay of theory and experiment, which is beginning to enable a rational design of optimized plasmonic nanostructures.

In this review, we highlight some of the key advances in each of the areas of fabrication, characterization, and understanding of NP plasmons. We emphasize the basic physical understanding and experimental techniques that will enable a new generation of applications, leaving detailed discussion of such applications to other reviews. This review is necessarily incomplete, and we encourage the reader to consider it as a starting point for understanding plasmons in metal NPs.

2. Fabrication

To characterize, understand and exploit metal-NP plasmonics, structures must be made reliably and routinely. Fabrication of metal NPs follows one of two approaches, commonly labeled as "top-down" and "bottom-up." The top-down method builds on the sophisticated microfabrication methods that have been developed over decades for the semiconductor industry [32]. The bottom-up method builds upon growth and self-assembly techniques developed in chemistry and biology. We will first discuss top-down techniques for NPs, then discuss bottom-up approaches, and will end with a discussion of fabrication for arrays and other complicated structures of NPs.

2.1. Lithographic approaches

The most common micropatterning technique is optical lithography; however, it is very difficult to expose features significantly smaller than the wavelength of light used, and the nanometer length scales required for plasmonic particles are inaccessible. Electron-beam-lithography (EBL) can define significantly smaller features, and is the most commonly used technique for the top-down fabrication of metal nanostructures. To make structures by EBL, an electron-beam resist is first deposited on a substrate, and is then exposed by scanning a focused electron beam over the surface. Development of the resist removes the exposed portions. A metal layer is then deposited on the sample, and the remaining resist is subsequently dissolved in a solvent, so that the metal deposited on the unpatterned part of the samples is removed. The great advantage of this technique is that it allows the production of relatively large numbers of nanostructures with a variety of different shapes. Although the structures are necessarily "flat" (e.g., EBL can produce disks but not spheres), nearly arbitrary 2D patterns can be created. The technique has been used to make arrays of disks [33], dimers of disks (see Fig. 1) [34], "bowtie" structures [35], and other shapes, with varying interparticle spacing.

An alternative top-down technique is focused-ion-beam (FIB) etching [36]. In this method, a continuous metal film is first deposited on a substrate. A highly energetic, tightly focused beam of ions is then accelerated towards the sample. The ions selectively sputter away material at their focus, and thus can form arbitrary 2D metal nanostructures. However, since the process involves the removal of material and is relatively slow, it is better suited to the production of holes in metal films than isolated metal NPs [37].

Novel lithographic techniques have recently been investigated for the definition of metal-NP arrays. For example, a technique dubbed "soft interference lithography" has been used to define ordered arrays of NPs with dimensions on the order of 100 nm, over areas from 1 μm^2 to more than 10 cm^2 [38, 39]. This method can overcome the relatively slow, serial processing of EBL and FIB, allowing for the production of metal NPs in much greater quantity.

2.2. Colloidal synthesis

Despite the sophistication and flexibility of lithographic techniques, difficulties remain in obtaining the high-quality metal nanostructures that are needed for exploitation of plasmon effects. It is highly challenging to use EBL or FIB to produce features with dimensions below 5 nm–10 nm. It

© 2008 by WILEY-VCH Verlag GmbH & Co. KGaA, Weinheim

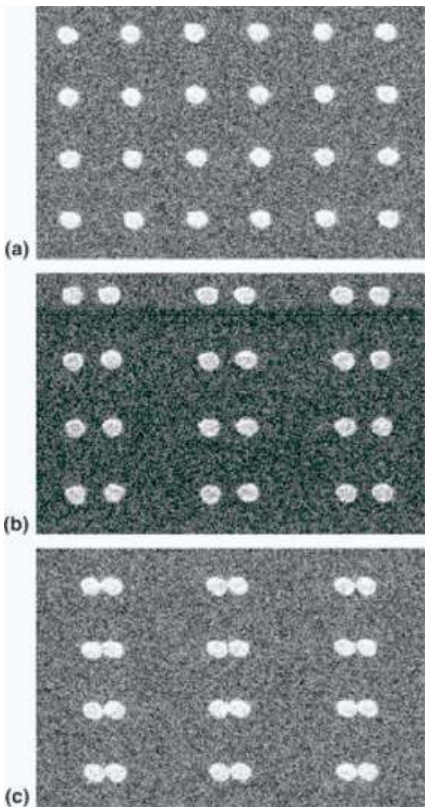

Figure 1 Scanning-electron-microscope images of particle pairs produced by electron-beam lithography, metal evaporation, and liftoff. The particles have diameters of 150 nm, heights of 17 nm, and center-to-center distances of (a) 450 nm, (b) 300 nm and (c) 150 nm. Reprinted from [34], Copyright (2003), with permission from Elsevier.

is thus difficult to obtain the sharp corners and nanometer-scale interparticle spacings that are of greatest interest in NP plasmonics. In addition, the use of metal evaporation results in particles that consist of multiple crystal domains, whose size, orientation, and arrangement are not well controlled. This, in turn, leads to roughness on the NP surfaces and variations in their sizes and shapes. To achieve greater control over the atomic-scale structure of metal NPs, the complementary technique of colloidal synthesis has been extensively pursued.

Colloidal gold solutions, stable and red colored, were prepared as early as the sixteenth century, and were believed to have great value as medicines. Michael Faraday made one of the first systematic studies of the unusual color of these solutions, in the mid-nineteenth century [40]. By reducing gold chloride in water with phosphorus or other reducing agents, he produced a "beautiful ruby fluid," and made several clever tests to support his idea that the color was due to a suspension of very small gold particles.

These colloidal solutions continued to attract attention over the years, but rapid developments occurred only in the mid-twentieth century, following the introduction of electron microscopy. With this new technology, researchers were able to make a systematic study of the NPs produced by different processes [41], and reduction of gold chloride with sodium citrate was identified as a particularly reproducible method of producing NP solutions with relatively uniform diameters. Separate control over the processes of nucleation and growth was obtained by careful adjustment of reagant concentration, and was shown to provide control over the average particle size while maintaining good monodispersity [42]. The gold particles produced by this citrate method are negatively charged, and it is this charge that leads to their stability in solution. Addition of salt or evaporation of the solvent leads to aggregation of the particles. If, by contrast, NPs are synthesized in the presence of capping ligands, the particles can be stabilized by binding of the ligands to the NPs, preventing aggregation [43]. As well, growth of the NPs is controlled by the surface coverage of the ligands, allowing for precise tuning of the particle diameter [44].

Moreover, the use of capping molecules provides a method for the anisotropic growth of NPs, allowing shapes other than spheres to be controllably synthesized. The capping agents can preferentially adsorb on certain crystal facets, so that the metal growth proceeds more quickly from other crystal faces, and the final NP shape reflects the geometry of these facets [45]. In the "polyol" process, for example, silver nitrate is reduced at high temperature by ethylene glycol, which also serves as the solvent. The use of polyvinylpyrrolidone (PVP) as a capping agent leads to highly non-spherical silver particles, such as the single-crystal nanocubes shown in Fig. 2 [46]. Additional control over the NP shape can be obtained by separating the nu-

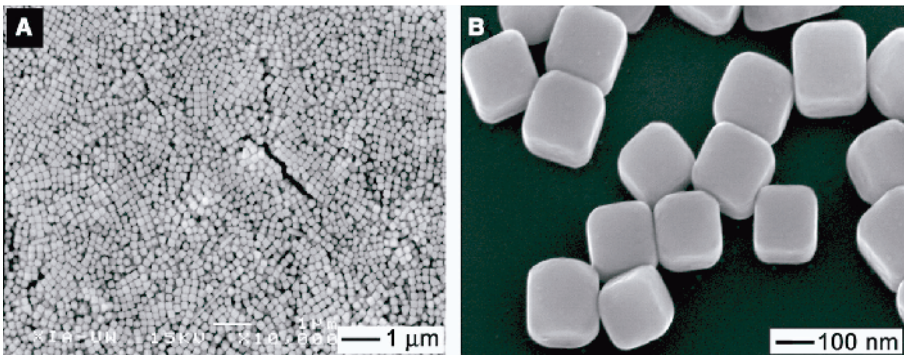

Figure 2 Scanning-electron-microscope images of silver nanocubes produced by the reduction of silver nitrate with ethylene glycol in the presence of polyvinylpyrrolidone. From [46]. Reprinted with permission from AAAS.

© 2008 by WILEY-VCH Verlag GmbH & Co. KGaA, Weinheim

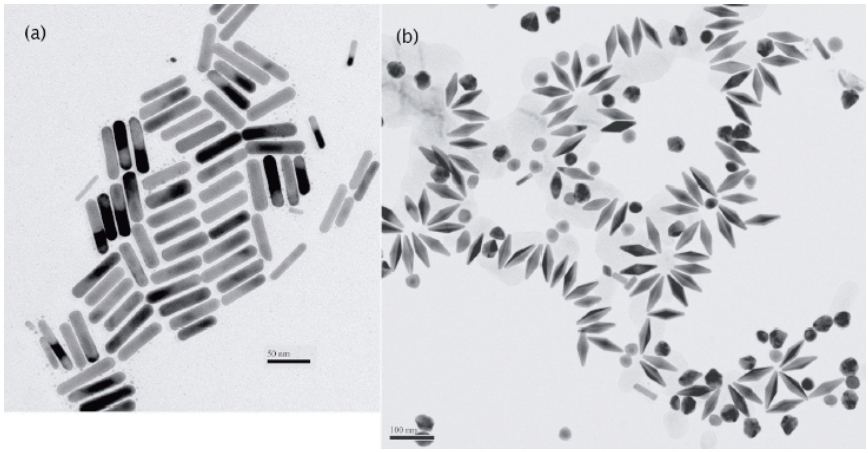

Figure 3 Transmission-electron-microscope images of (a) gold nanorods and (b) gold bipyramids produced using a seed-mediated growth process. For growth of rods, single-crystal seeds are produced by reducing $HAuCl_4$ with $NaBH_4$ in the presence of cetyltrimethylammonium bromide (CTAB). For the bipyramids, a sodium-citrate-based reduction method is used to produce multiply twinned seeds. The particles are grown from these seeds using ascorbic acid as the reducing agent, in the presence of CTAB and of silver ions, at pH = 3. Figure courtesy of M. Liu.

cleation and growth processes: small, spherical NPs are first nucleated using a standard reduction process, and these seeds are then grown into larger, anisotropic particles through a slower reduction process in the presence of a capping molecule. For example, the polyol process described above could be modified by dividing the reduction process into two steps, the first one involving the formation of seed NPs, and the second one involving anisotropic growth from those seeds; in this way, very long silver nanowires were produced [47, 48].

A different seed-mediated growth process has been used to produce rod-shaped gold and silver NPs [49–52]. Fig. 3(a) shows an image of gold nanorods produced using a seed-mediated method [53]. This technique can produce atomically smooth surfaces, controllable aspect ratios, and better than 95% yield. Moreover, the shape of the NPs can be changed by altering the crystal structure of the seeds. For example, starting with multiply twinned seeds, rather than the single-crystal seeds used to produce nanorods, leads to bipyramidal particles, as shown in Fig. 3(b). The bipyramids show a remarkable uniformity in their shape and have sharp tips, making them attractive for the the enhancement of local fields. Starting with larger twinned seed particles leads to more complex, star-shaped gold NPs; these nanostars are approximately 100 nm in size and can have from one to seven sharp points [54]. Finally, it is possible to overcoat gold nanorods after growth with nanometer-scale layers of silver. The silver shell leads to a blue shift in the resonance wavelength of the NP plasmons; by varying the shell thickness, a wide range of colors can be obtained, as shown in Fig. 4. Using a different technique, gold shells can be overgrown on SiO_2 cores, producing plasmon resonances widely tunable via the shell dimensions [30].

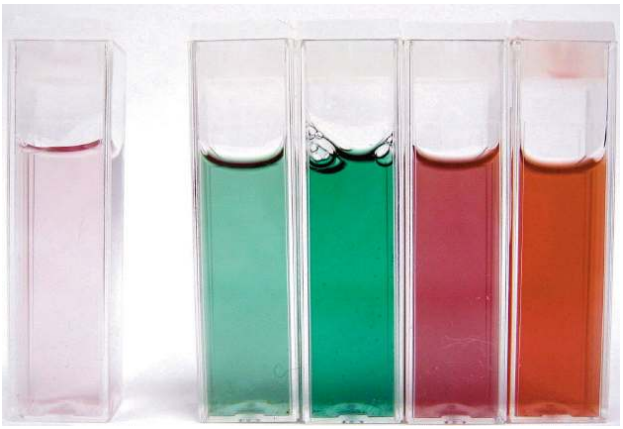

Figure 4 (online color at: www.lpr-journal.org) Aqueous solutions of gold and gold-silver nanorods. The leftmost solution contains gold nanorods; the other solutions, from left to right, contain gold nanorods overcoated with silver shells of increasing thicknesses. Core-shell structures were obtained by first stabilizing the nanorods with PVP, and then reducing $AgNO_3$ with ascorbic acid; NaOH was used to increase the pH of the solution and enable the reduction process. Figure courtesy of M. Liu.

2.3. Self assembly

Compared to structures that can be fabricated using top-down methods, the chemically synthesized NPs have the advantage of being single crystals with nearly atomically smooth surfaces. The tradeoff for this improved material quality is the difficulty of arranging colloidal NPs into desired configurations. Unlike lithographic particles, which can be made into any arbitrary pattern, chemically-synthesized particles are randomly distributed in solution. A current challenge that must be overcome before many of the applications of metal NPs can be realized is the development of assembly methods that can be used to order the particles into complex patterns.

One such assembly method is based on Langmuir-Blodgett techniques, which have long been studied for the assembly of molecular monolayers. A small volume of NPs in organic solvent is dispersed on water. As the solvent evaporates, a sparse monolayer of the NPs forms on the water surface. The monolayer is then compressed by sliding a barrier across the surface. Under the right condi-

© 2008 by WILEY-VCH Verlag GmbH & Co. KGaA, Weinheim

tions, a close-packed monolayer of NPs is formed [55]. The monolayer can subsequently be transferred intact to various substrates by lifting the substrate through the surface layer. This technique has recently been generalized to a variety of different NP shapes, each resulting in a different packing geometry [56].

An alternative method for the production of ordered NP films involves controlled evaporation of the solvent containing the NPs. For example, highly ordered two-dimensional layers of gold NPs have been obtained through self-assembly at the liquid-air interface of a rapidly evaporating droplet [57, 58].

A technique that has come to be known as "nanosphere lithography" [59] combines bottom-up and top-down methods. An ordered, two-dimensional layer of polymer spheres is assembled on a substrate by precipitation out of solution. Metal is then deposited on the entire surface, and the spheres are subsequently dissolved in solvent, leaving behind a metal pattern on the surface that is an image of the gaps between the spheres [60]. Since the spacings between the spheres are smaller than the diameters of the spheres, micrometer-scale polymer spheres can be used to define periodic arrays of metal particles with dimensions of hundreds of nanometers. A modification of this technique involves ion beam etching after deposition of the metal film; the etch removes the film between the spheres, while secondary sputtering creates a metal shell around the spheres. Subsequent removal of the spheres thus results in free-standing metal rings [61].

Despite their elegance, self-assembly methods can lead only to relatively simple, periodic structures. As well, it is difficult to avoid the existence of defects and to achieve large-scale ordering using such techniques. To reach the goal of creating arbitrary arrangements of metal NPs with nanometer-scale control over interparticle spacing, it will be necessary to develop novel, hybrid methods. One such approach that has recently been explored is to guide evaporation-driven self-assembly using patterned substrates [62, 63]. Standard lithographic techniques are used to pattern a series of indentations or trenches onto substrates, and NPs are deposited on the substrates using controlled evaporation. A combination of local pinning of the liquid contact line and capillary forces induce deposition of particles only in the trenches, as illustrated in Fig. 5. Development of this method has the promise to allow colloidal particles to be deposited at a desired location and with a desired orientation on an arbitrary substrate.

An alternative is to use selective chemical functionalization to guide self-assembly processes. For example, the seed-mediated growth of rods proceeds because the surfactant protects the side faces better than the end faces; this same selectivity can be used after the rods have been grown to bind functional groups to their ends. Using biotin, a small biomolecule, as the functional group, and adding, streptavidin, a protein that has a strong affinity for biotin, to the nanorod solution, the rods were induced to largely assemble end-to-end [64]. A similar approach involves the selective functionalization of the ends of rods

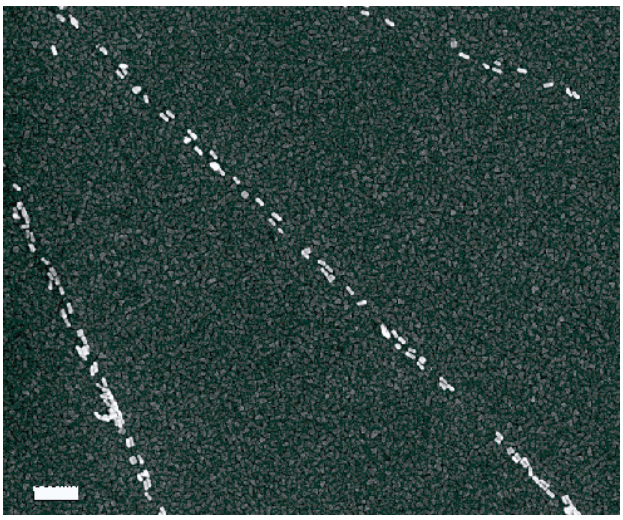

Figure 5 Gold nanorods arranged by an evaporation-driven guided self-assembly process. The scale bar is 300 nm. Electron-beam lithography was used to define trenches, approximately 40 nm wide. The patterned substrate was rendered partially hydrophilic by treating with an oxygen plasma, and was then placed in a dilute nanorod solution. As the solution evaporated, the contact line moved down the sample, leaving behind particles in the trenches.

with carboxylic acid derivatives, which assembles the rods end-to-end by hydrogen bonding [65]. Recently, the ends of rods were selectively functionalized with polystyrene, rendering them hydrophobic, while the center portions of the rods remained hydrophilic due to their CTAB coating [66]. By adding water to a solution of these nanorods in organic solvents, the rods were induced to organize in different, controllable arrangements, including end-to-end chains, side-to-side bundles, and hollow spheres. Furthermore, the spacings between rods assembled end-to-end could be tuned simply by changing the amount of water added to the solutions.

3. Optical characterization

The ability to controllably fabricate and assemble metal NPs must be accompanied by an accurate understanding of how they interact with light. The extinction spectra of ensembles of metal NPs have been studied for many years. However, any ensemble contains a distribution of particle sizes and shapes, making it difficult to obtain a detailed correspondence between the NP structure and its optical response. To reveal the inherent optical response of metal NPs, then, it has become necessary to study single particles. In this section, we discuss methods used to measure the optical properties individual NPs and review the general conclusions that can be drawn from such measurements. We also discuss recent attempts to probe the nonlinear optical properties of metal NPs.

© 2008 by WILEY-VCH Verlag GmbH & Co. KGaA, Weinheim

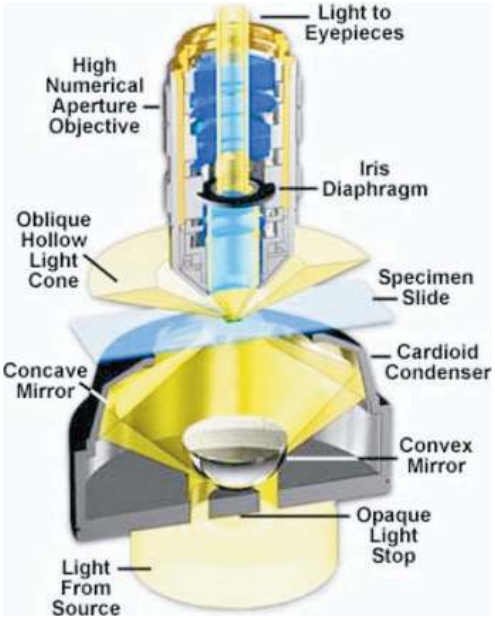

Figure 6 (online color at: www.lpr-journal.org) Schematic of illumination and light collection in a typical darkfield microscope. A high numerical-aperture condenser lens is used to illuminate the sample. An annular beam stop before the condenser blocks the center portion of the illuminating beam, so that light is incident on the sample only at high angles. A lower numerical-aperture objective lens is used for imaging, so that any light directly passing through the sample is not collected by the objective. Light scattered by the sample into lower angles is collected and imaged by the microscope. Figure reprinted with permission from Michael W. Davidson and The Florida State University Research Foundation.

3.1. Linear response

Optical studies of single metal NPs started in 1903, when Zsigmondy developed the "ultramicroscope" for his studies of colloids [67]. The instrument illuminated particles in solution with an intense beam of light, and light scattered off the particles in the perpendicular direction was collected using an objective lens. Individual particles could be seen as bright flashes against a dark background, as they diffused through the illuminating beam. This technique eventually led to modern darkfield microscopy, as illustrated in Fig. 6. Darkfield illumination and wavelength-resolved detection of scattered light allows for the routine measurement of the scattering spectra of single metal NPs [68, 69]. The same sample can later be imaged by electron microscopy, allowing for a detailed comparison between individual NP structure and scattering spectra [70].

Closely related to the technique of dark-field microscopy is evanescent excitation, or total-internal-reflection microscopy [71]. The particles are placed on the top surface of a glass prism, and illumination light is sent through the prism so that it is incident on the surface at an angle beyond the critical angle for total internal reflection. A microscope objective above the prism is used to collect light. As in the case of dark-field illumination, very little background light enters the objective, and the only signal collected is due to scattering off individual NPs.

A different approach to probing individual metal NPs is near-field scanning optical microscopy (NSOM) [72]. The most common form of NSOM involves scanning a metal-coated, tapered fiber tip in nanometer-scale proximity to the sample surface. In illumination-mode NSOM, laser light is coupled through the fiber, and passes through a small aperture, typically 50 nm or less in diameter, at the end of the tip. This light then scatters off the NPs and is collected in the far field. By tuning the wavelength of the illuminating laser, it is possible to determine the scattering spectra of individual particles [73]. An alternative geometry, known as collection-mode NSOM, involves illuminating the sample over a large area, and collecting light through the small fiber aperture. The more recently developed "apertureless" NSOM involves scanning a sharp probe, such as an atomic-force-microscope tip, above an illuminated sample, and collecting the small fraction of light that is scattered off the probe [74, 75]. All these techniques are able to achieve resolutions of 50 nm or better, well beyond the resolving power of a far-field optical microscope. They can thus be used to investigate densely packed samples and can gain direct information about the near fields of the particles. The tradeoff for this improved resolution is a significantly more complex experimental arrangement; in addition, interaction between the scanning-probe tip and the particle being studied complicates the interpretation of the measured signal.

From the many measurements that have been performed using these various techniques, a consistent picture has emerged for the linear optical response of metal NPs with relatively simple shapes. For diameters in the range of approximately 10 nm to 50 nm, known as the "quasi-static" regime, the plasmon resonance frequency and linewidth is nearly independent of the particle size; on the other hand, the resonance is highly sensitive to the shape of the particle. The plasmon resonance of gold nanospheres with these diameters is at a wavelength of approximately 520 nm and is broad, due to the relatively strong optical absorption of gold in this spectral region. For silver spheres, the resonance is at approximately 440 nm, and the linewidth is narrower. As we discuss in Sect. 4.2, one of the simplest geometries that allows for tuning of the plasmon resonance is a rod-shaped NP. In this case, the plasmon resonance splits into two: a transverse plasmon, corresponding to oscillation of electrons along the short axis of the rod, and a longitudinal plasmon, corresponding to oscillation along the long axis of the rod. Although the transverse plasmon has approximately the same wavelength as the plasmon in spheres, the longitudinal plasmon shifts to longer wavelengths as the aspect ratio of the rods increases. For gold rods, in particular, this can move the resonance to regions where the optical losses are lower, thereby significantly reducing damping and decreasing the linewidth [69]. Forming a silver shell around the gold rods, on the other hand, shifts the longitudinal plasmon resonance to shorter wavelengths, as illustrated in Fig. 7 [76].

© 2008 by WILEY-VCH Verlag GmbH & Co. KGaA, Weinheim

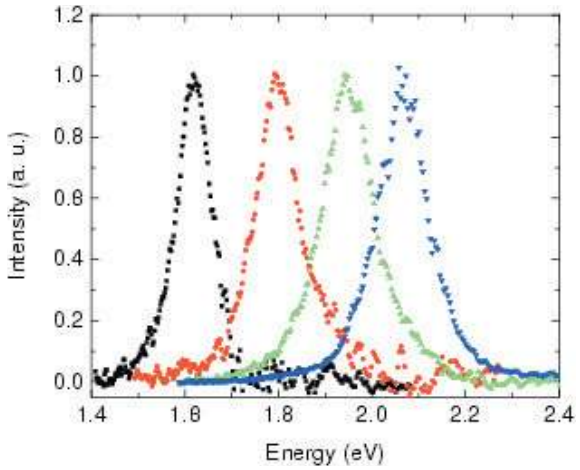

Figure 7 (online color at: www.lpr-journal.org) Scattering spectra of single gold and gold-silver nanorods measured using evanescent illumination. The leftmost spectrum is for a gold nanorod; the other spectra, from left to right, are for gold nanorods overcoated with silver shells of increasing thicknesses. Figure courtesy of M. Liu.

In Sect. 4.2, below, we explain how the plasmon resonance depends on the geometry of nanorods. One conclusion is that the quasi-static approximation is valid only for a very limited range of nanorod dimensions. Higher-order effects contribute for larger particles, red-shifting and broadening the plasmon resonances. On the other hand, for particles with dimensions less than approximately 10 nm, the plasmon linewidth again broadens, reflecting deviations of the material response from that of the bulk metals. These size-dependent effects are less well understood; in particular, little is known about the crossover from the plasmonic response of nanometer-scale metal particles, which contain several hundreds or thousands of atoms, to the molecule-like response of small clusters of less than 100 atoms.

The techniques described above, though, are generally unable to resolve the response of such small particles, because the scattering cross-section of NPs scales as the square of their volume. A number of techniques have therefore been developed in recent years to enhance the signal-to-noise ratio for single-particle measurements, allowing the minimum detectable particle size to be significantly reduced. One such approach is to measure the optical absorption of individual NPs. Since the absorption cross-section is proportional to the NP volume, it does not fall off as dramatically for decreasing particle diameter. Nonetheless, the cross-section of a 5-nm gold particle is about five orders of magnitude smaller than the diffraction-limited spot size of a focused laser in a high-power microscope, so that some form of signal enhancement is necessary to directly measure the NP absorption. Vallée and co-workers have developed a technique where the NP is rapidly oscillated over a few hundred nanometers within the laser spot, and the resulting modulation in the transmitted light is then detected using a lock-in amplifier [77, 78].

Another method to improve contrast is to interfere the light scattered off the particle with a reference optical beam. In one such "heterodyne" scheme, individual NPs were illuminated with broadband light in an illumination-mode NSOM; in this case, the local oscillator was simply the portion of the light directly transmitted by the sample that did not scatter off the particle [79, 80]. Another, closely related method involves far-field illumination of a particle on a substrate, using a standard microscope objective, and detection of the reflected light; in this case, the interference is between light scattered off the particle and reference light reflected off the surface of the substrate [81]. Finally, the technique of differential interference contrast (DIC), commonly used in microscopy to enhance contrast in imaging of transparent samples, has also been used to characterize single metal NPs [82]. In this technique, the incident illumination is split into two orthogonally-polarized components, which are focused onto two closely-spaced spots on the sample. A single NP is located at one of the two spots, and the other spot serves as the reference. Light returning from the sample is recombined, resulting in interference between the signal and reference beams.

A unique method involves the indirect measurement of the optical absorption of single NPs, by probing the heating of their surroundings [83]. A first laser pulse, resonant with the particle plasmon, is absorbed by the particle, leading to local heating of the environment. A second, non-resonant laser is used in a DIC-like configuration to measure changes in the refractive index of the heated medium. To further improve signal-to-noise, the heating laser is modulated rapidly, and lock-in detection of the probe laser is employed. This method has the particular advantage that it is insensitive to scattering by non-absorbing material in the vicinity of the NP being probed. The sensitivity of this photothermal technique was improved by replacing the DIC probe configuration with a far-field heterodyne configuration [84]. By tuning the wavelength of the heating beam, the absorption spectra of individual gold NPs with diameters down to 5 nm could be resolved [85, 86]. This clearly revealed that the plasmon resonance shifts to shorter wavelengths and broadens as the size of the NP decreases. The increasing linewidth is not predicted by theories that involve the bulk optical properties of gold, verifying the existence of an inherent size-dependent effect. This, in turn, has generally been explained by invoking a damping of the plasmons by the NP surfaces, but the microscopic validity of this model remains to be determined.

3.2. Nonlinear response

Developing a more detailed understanding of the interaction of light with metal NPs requires going beyond the linear response described above. Since optical fields are strongly confined within and around NPs, nonlinear interactions can be greatly enhanced. For example, second-order nonlinearities depend on the fourth power of electric fields, meaning that enhancement factors should be considerable.

© 2008 by WILEY-VCH Verlag GmbH & Co. KGaA, Weinheim

Such nonlinearities are most commonly studied through second-harmonic generation (SHG); however, the dominant dipole contribution to SHG is cancelled in the case of centrosymmetric particles, such as spheres and rods. This symmetry can be broken by accumulating gold nanoparticles at a liquid-liquid interface; in this case, strong SHG signals were observed when the generated harmonic is resonant with the plasmon oscillation [87]. Alternatively, electron-beam fabrication can be used to produce nanoparticles that do not exhibit centrosymmetry [88]. The SHG signal from such particles was used in an autocorrelation configuration to directly measure the dephasing time of nanoparticle plasmons. This technique was later extended to the study of single nanoparticles [89]. Other measurements extended this technique by using third-harmonic generation (THG) instead, thereby allowing centrosymmetric particles to be studied [90]. Recently, THG signals have been obtained from single gold nanoparticles [91]. Since essentially all materials generate third-harmonic radiation, this observation required careful separation of the weak single-particle signal from the large background coming from the substrate on which the particles rested.

Such THG measurements provide information about inherent third-order nonlinearities of metal nanoparticles. Complementary, time-resolved measurements can be obtained using techniques such as four-wave mixing [92–94] and transient transmission [95]. The latter method, in particular, has been studied extensively, because of its ability to reveal the fundamental properties of NP plasmons under strong excitation and of the ultrafast dynamics of electrons in the NPs. In such measurements, an intense "pump" laser pulse, usually 100 fs or less in duration, is focused into a NP solution. After a certain delay, a second, weaker "probe" laser pulse is transmitted through the same part of the sample. The transmission of the probe is measured, and the process is repeated for a series of pump-probe time delays, allowing for the measurement of the temporal response of the NPs. The probe typically covers a broad spectral band, allowing the response to be resolved in wavelength as well as in time.

Over the past decade, many such experiments have been carried out, and a detailed understanding of the nonlinear response has been developed [96–99], as summarized in Fig. 8. The initial excitation of the NPs by a pump laser pulse results, on time scales less than 100 fs, in the creation of a highly non-thermal, energetic distribution of conduction electrons. The non-thermal distribution rapidly decays, in less than a picosecond, to a thermal distribution, through electron-electron scattering. Since the heat capacity of conduction electrons is low, the resulting electron temperature can be several thousand Kelvin for typical pump powers. The electrons then exchange heat with the lattice through electron-phonon coupling. Since the heat capacity of the conduction electrons depends on temperature, the decay of electron temperature is non-exponential and dependent on pump power, but is generally in the range of 1 ps to 5 ps. The temperature after this relaxation is typically on the order of 10 K higher than the initial temperature. At the same time, the lattice exchanges heat with its surroundings, reaching ambient temperature on a time scale that depends on the heat capacity of the environment and the thermal conductivity of the ligand molecules, but that is generally on the order of 100 ps. Superimposed on this lattice cooling is a back-and-forth expansion and contraction of the entire particle volume; this coherent breathing mode has a period on the order of 10 ps, depending on the size and shape of the particle. All these effects alter the dielectric function of the metal making up the particles, which, in turn, shifts and broadens the plasmon resonance. Detailed models have been developed for the dielectric constants of bulk silver and gold and their dependence on temperature [100–103], and these models are able to reproduce well the great majority of experimental observations.

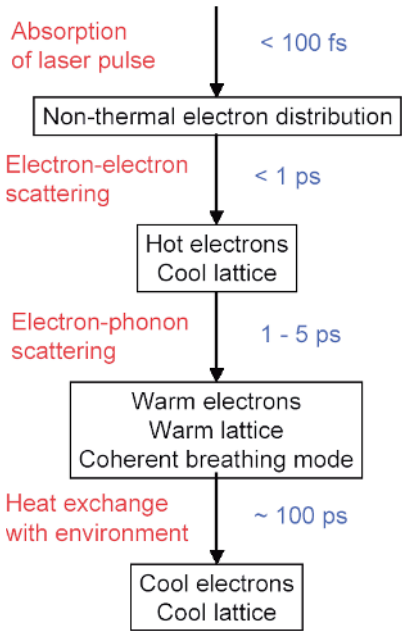

Figure 8 (online color at: www.lpr-journal.org) Flowchart of the processes involved in the response of a metal nanoparticle to an incident, intense laser pulse. Since the time scales involved are well separated, the processes can be considered as sequential.

A principal goal of studying the nonlinear properties of NPs, though, is to reveal dynamical effects that depend on their nanometer-scale dimensions. In particular, several attempts have been made to study the dependence of electron relaxation on NP size. Initial experiments on NPs in solution revealed no changes in relaxation rates for particle sizes down to 2.5 nm [104–106]. However, the somewhat limited signal-to-noise ratio in these experiments necessitated the use of relatively high-energy pump pulses, and the inherent size-dependent response may have been obscured by the pump-power dependence. A recent, higher-sensitivity set of experiments, on the other hand, has indicated a systematic increase in the rate of relaxation of high-temperature electrons as the diameter of gold and silver NPs is reduced below about 10 nm [107]. Contrary to

© 2008 by WILEY-VCH Verlag GmbH & Co. KGaA, Weinheim

previous reports [108, 109], no dependence on the environment of the particles was observed, so that the effects could be attributed to intrinsic properties of the NPs. Similar measurements also showed an increase in electron thermalization rate with decreasing NP diameter in the same size regime [110]. The measurements thus suggest increased electron-electron and electron-phonon scattering due to interaction with the NP surfaces. A simple model, based on reduced screening of electron-electron interactions near the particle surface, reproduced the experimental results qualitatively.

All of the above experiments have involved either exciting or probing the particles away from their plasmon resonances. Although the measurements can reveal information about electron dynamics in the particles, they cannot directly probe the nonlinear response of the plasmon resonances. This, by contrast, requires a wavelength-degenerate measurement, so that the pump and probe are both resonant with the plasmons [111]. This was recently attempted using gold nanorods similar to those in Fig. 3(a). As well as pump-probe transient-extinction measurements, four-wave mixing experiments were performed. In these measurements, two pump pulses are simultaneously incident from different directions on the sample. The overlapping pulses create an interference pattern, and interaction of this pattern with the sample leads to a spatially modulated complex refractive index. After a certain time delay, a probe pulse diffracts off this modulation and is detected. In this experiment, the diffracted signal was mixed with a local oscillator, allowing the real and imaginary part of the nonlinear response to be resolved [112]. The frequency shift and broadening of the plasmon resonance could thereby be separately determined, as shown in Fig. 9. The picosecond-scale cooling of heated conduction electrons is clearly visible in both the shift and broadening, as is the slower cooling of phonons. The coherent breathing-mode oscillations, on the other hand, are primarily visible in the frequency shift.

It is difficult to determine coherent, resonant responses from an ensemble measurement, because the optical response is broadened by the inhomogeneous distribution of particle sizes and shapes. Many particles are off resonance with the pump, and thus have nonlinear responses much smaller than or even opposite in sign to the resonant particles. By contrast, if single particles are isolated, the effects of inhomogeneity are removed and the quantitative measurement of inherent properties becomes possible. In addition, single-particle measurements make it possible to directly correlate the NP structure and its nonlinear response. This may make it possible to determine a more detailed correspondence between electron relaxation rates and particle size and shape, allowing more quantitative models to be developed [107, 110].

Dark-field microscopy, evanescent illumination, and near-field scanning optical microscopy all allow measurement of nonlinear scattering [113, 114]. It then becomes possible to make single-particle measurements of the resonant response on 20-fs time scales [115]. Surprisingly, although the ultrafast nonlinearity is large, corresponding

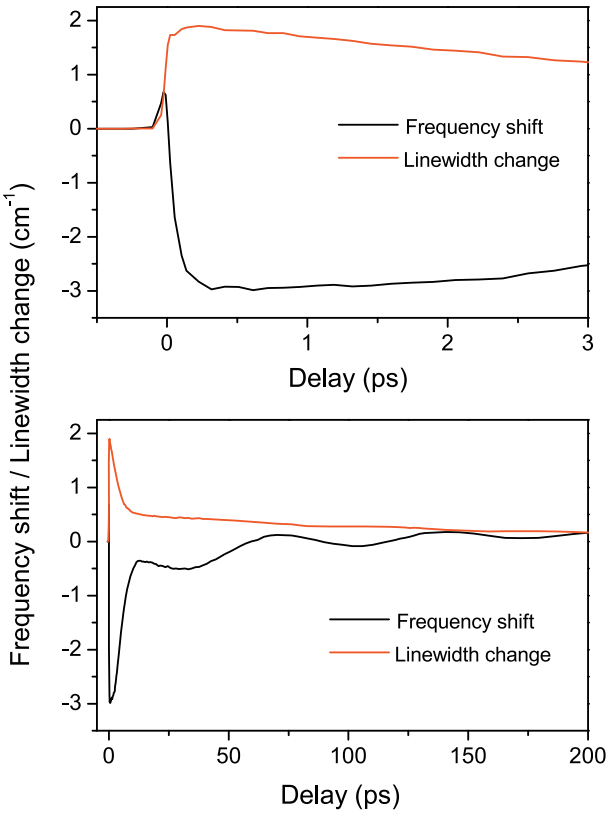

Figure 9 (online color at: www.lpr-journal.org) Time-dependent frequency shift and bandwidth change of plasmon resonances in ensembles of gold nanorods, as a function of time delay after pumping with a resonant laser pulse. The results are determined from experimental data obtained by optical-heterodyne-detected four-wave mixing. From [111].

to as much as 20% of the linear scattering, its magnitude is identical to that due to thermal effects. This is illustrated in Fig. 10(a), where the light from an incident laser, scattered by a single gold nanorod, is resolved spectrally. The broadening of the scattering spectrum is consistent with the assumption that the only effect of the incoming light is to instantaneously heat conduction electrons, as shown in Fig. 10(b). This strongly suggests that the plasmons lose their coherence on a time scale much shorter than the 20-fs duration of the laser pulses, indicating a previously unrecognized induced damping of plasmons in metal NPs.

Although these measurements were able to reveal a novel plasmon saturation, their signal-to-noise ratio was limited. More sensitive measurements can be achieved using the various signal-enhancing techniques described in the previous section [116]. For example, spatial modulation and lock-in detection allow high-quality transient-absorption measurements to be made on individual silver NPs with diameters down to 21 nm [117]. In an alternative implementation, the probe pulse is supplemented by a second, reference pulse polarized orthogonally to the probe and delayed by 10 ps [118, 119]. After passing through the

© 2008 by WILEY-VCH Verlag GmbH & Co. KGaA, Weinheim

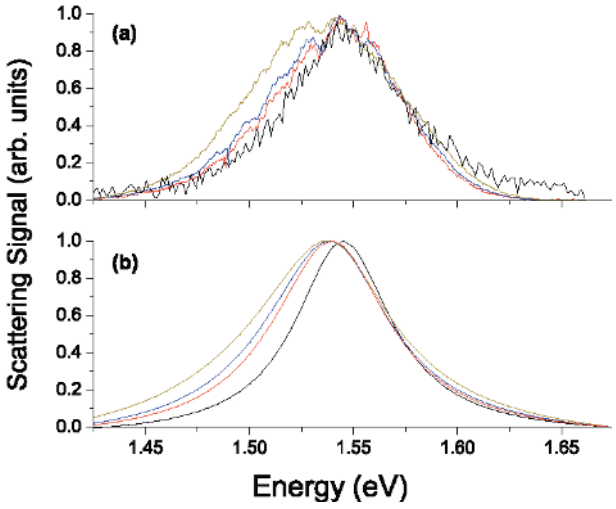

Figure 10 (online color at: www.lpr-journal.org) (a) Measured scattering spectra from single gold nanorods for different incident laser intensities. The black curve is the linear spectrum measured using incoherent, broadband excitation. The other curves are measured using a 20-fs laser pulses with energies of 52 pJ, 82 pJ, and 192 pJ, from right to left. The curves are normalized for ease of comparison. (b) Corresponding calculated scattering spectra, assuming spectral changes are due solely to instantaneous heating of conduction electrons. From [115].

sample, the reference and probe are overlapped and interfere with one another, allowing for the detection of small changes in the amplitude of the probe. This technique has been used to resolve the nonlinear response of individual gold particles with diameters down to 40 nm. Acoustic oscillations have been observed to persist for up to 200 ps, revealing the inherent damping that was previously obscured by inhomogeneous broadening in the ensemble. Interpretation of the data is difficult, though, because of the relatively long delay between the probe and reference pulses.

Reaching an understanding of inherent plasmonic nonlinearities will have important consequences for applications. The great majority of applications, including surface-enhanced Raman scattering, biological sensing, and fluorescence enhancement, rely on achieving strong electromagnetic near fields around the particles. The substantial nonlinear response, though, will limit the magnitude of the local fields that can be achieved in practice. On the other hand, the nonlinearity serves to transform the metal NPs from passive to active elements. A strong, ultrafast nonlinearity could potentially be employed for high-speed, all-optical switching on the nanometer scale, leading to a new class of functional photonic devices.

3.3. Coupling to emitters

So far, we have treated metal NPs in isolation. Although this already reveals many interesting and important phenomena, the greatest promise for these objects will lie in coupling them to other types of materials. In particular, the highly localized fields that arise when plasmon resonances are excited should allow for strong coupling of the plasmons to excitations in light-emitting materials. Enhancement of luminescence from emitters such as organic dye molecules and semiconductor nanocrystals is of considerable practical interest for the improvement of light-emitting devices as well as the development of novel fluorescence imaging techniques, and may lead to novel physical phenomena, such as nanoscale lasing and formation of quantum-mechanical hybrid exciton-plasmon modes. Understanding the coupling between NPs and emitters is a challenge, though, because several competing phenomena occur simultaneously as they are brought together: (1) absorption of the excitation light by the emitter is enhanced; (2) radiative emission rates are increased; and (3) non-radiative energy transfer from the emitter to the metal is increased. The first two effects serve to enhance the overall emission rate, while the third serves to quench it. All three depend strongly and differently on the separation between the metal NP and the emitter, as well as the detuning between the plasmon resonance and the absorption and luminescence wavelengths of the emitter, the shape of the NP, and the orientation of the emitter's dipole moment. In addition, coupling to the metal NP can modify the spatial pattern of emission, so that the fraction of light captured in a particular experimental configuration can change.

Studies of plasmon-enhanced luminescence began with random collections of NPs, deposited as rough films on surfaces [120]. Average luminescence intensities from adsorbed dye molecules could be increased by over an order of magnitude, which was attributed primarily to increased absorption of the excitation laser by the molecules. Time-resolved measurements showed that excited-state lifetimes of the dye molecules decreased by more than two orders of magnitude, due primarily to a non-radiative energy transfer process [121, 122]. More recently, semiconductor nanocrystals, or quantum dots (QDs), have been used instead of dye molecules, in order to take advantage of their lower photobleaching and larger transition dipole moments [123, 124]. By monitoring individual QDs on random metal films, five-fold increases in emission intensity were observed, together with an increase in recombination rate that can be over a factor of 1000, as illustrated in Fig. 11 [125–127].

Quantifiable and reproducible results have been limited, though, because of the random nature of the NP films. The particles are widely distributed in size and shape and are strongly coupled one to another, leading to a broad and heterogeneous optical response. The gaps between the particles are variable, leading to a wide distribution of distances between the metal surfaces and the molecules or quantum dots. As well, it is difficult to ensure that the density of dye molecules remains the same for different samples, since the surface area can change considerably. Even if single-emitter measurements are made, the local structure of the metal around the location of the emitter is not known.

A first step towards remedying these difficulties is to chemically synthesize a monodisperse ensemble of sepa-

© 2008 by WILEY-VCH Verlag GmbH & Co. KGaA, Weinheim

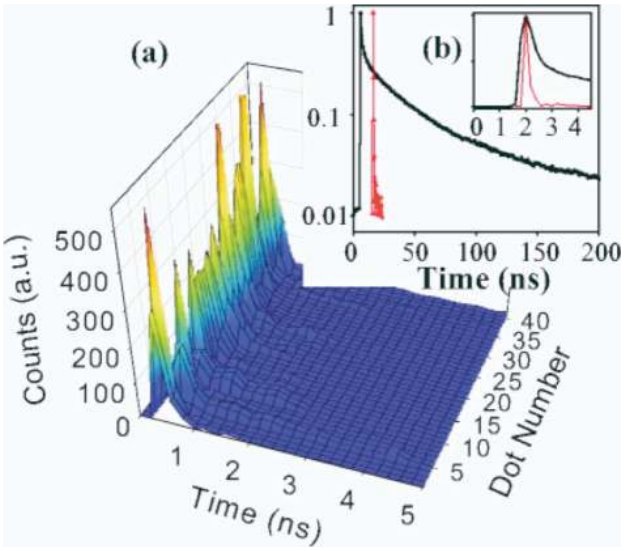

Figure 11 (online color at: www.lpr-journal.org) (a) Emission intensity as a function of time after excitation, for 40 individual quantum dots on a rough metal surface. (b) Time-dependent emission from a single dot on the metal film and from an ensemble of dots in the absence of the metal (black). In the main panel, the two curves are offset in time for clarity. Reprinted figure from [125], Copyright (2002) by the American Physical Society.

rated metal NPs in solution and then to chemically bind emitters to each NP. Well-defined separations between the metal and emitters can be obtained by using specific linker molecules, such as organic molecules [128] or short strands of DNA [129–132], or by coating the metal NPs with thin shells of silica [133, 134] or polymer [135]. Strong quenching of fluorescence was seen for various fluorophores attached to 1.4-nm or 2.5-nm diameter gold NPs [129, 130]. The efficiency of this quenching was observed to scale as $1/d^4$, when the distance d between the fluorophore and the center of the NP was varied up to 25 nm [131]. In different measurements, fluorescence intensities and lifetimes were measured as the size of the metal NP or the distance between the NPs and dye molecules was changed, and the results were interpreted as indicating that the quenching is largely due to an decrease in the radiative emission rate from the molecules [128, 132, 135]. Using larger NPs that demonstrate a clear plasmon resonance and emitters that are resonant with those plasmons, it was possible to observe both enhancement and quenching of fluorescence, depending on the separation between the metal NPs and emitting molecules or quantum dots [133, 134]. Quantitative interpretation of all these experiments, though, is complicated by limited knowledge about the fraction of molecules bound to the metal NPs and the total number or concentration of dye molecules studied. Interpretation also requires the assumptions that excitation and collection efficiencies are identical for different samples and that all molecules and NPs are treated identically, so that heterogeneities, particularly in molecular orientation, are not taken into account. Also not accounted for are interactions among the molecules bound to the NP surfaces, which may vary with NP diameter.

Rather than attaching several emitters to a single metal NP, a complementary approach involves attaching several small metal NPs to a larger semiconductor nanocrystal. For example, gold NPs, 1.4 nm in diameter, were bound to quantum dots using polypeptide chains, allowing a systematic study of the quenching efficiency as a function of separation between the two materials [136]. Quantitative agreement, once again, was not obtained between experimental results and any of the theoretical models considered. This may, similarly, be partially attributed to unknown characteristics of the sample, such as the exact number and distribution of gold particles bound to each quantum dot and interactions among the gold particles. In different experiments, small gold or silver particles were attached to long semiconductor nanowires using biotin-streptavidin pairs, forming a dense shell around the nanowires [137, 138]. In this case, emission from the wires was enhanced by as much as a factor of five, accompanied by a moderate increase in emission rate. For gold NPs, enhancement was attributed primarily to enhanced radiative rates, whereas, for silver NPs, it was attributed to enhanced absorption of excitation light. However, the detailed arrangement of the NPs is random and variable from rod to rod, making it difficult to develop a quantitative model for the system.

As in the case of the linear and nonlinear spectroscopy of metal NPs alone, single-particle measurements can remove structural inhomogeneities, opening up the potential for quantitative comparison of the structure of coupled NPs and emitters and their optical properties. The first step in this direction is a straightforward extension of the ensemble measurements described above: emitters are chemically bound, with controlled spacing, to colloidal metal NPs, and single particles are then isolated and studied optically. In particular, 1.4-nm gold NPs were bound to single quantum dots using short strands of DNA [140]. By varying the length of the DNA spacer, the distance dependence of the QD fluorescence quenching was verified. In separate experiments, various dye molecules were bound with DNA to larger metal NPs, which had different shapes, and thus different plasmon resonance frequencies [139]. Darkfield microscopy was used to measure the scattering spectra of individual particles, as illustrated in Fig. 12(a), and fluorescence microscopy was used to measure the emission intensity from dye molecules attached to the same particles. As shown in Fig. 12(b, c), the fluorescence intensity was strongly correlated to the overlap between between the plasmon resonance of the NPs and the absorption and emission spectra of the dyes.

This measurement, though, still involves several dye molecules for each metal NP, so that differences in coverage of the metal NPs and interactions among the molecules may play a role. As well, several different NPs must be compared to obtain systematic results, and these NPs may have other properties, apart from their resonance frequency, that vary from particle to particle and influence how they couple to emitters. By contrast, a pair of recent experiments

© 2008 by WILEY-VCH Verlag GmbH & Co. KGaA, Weinheim

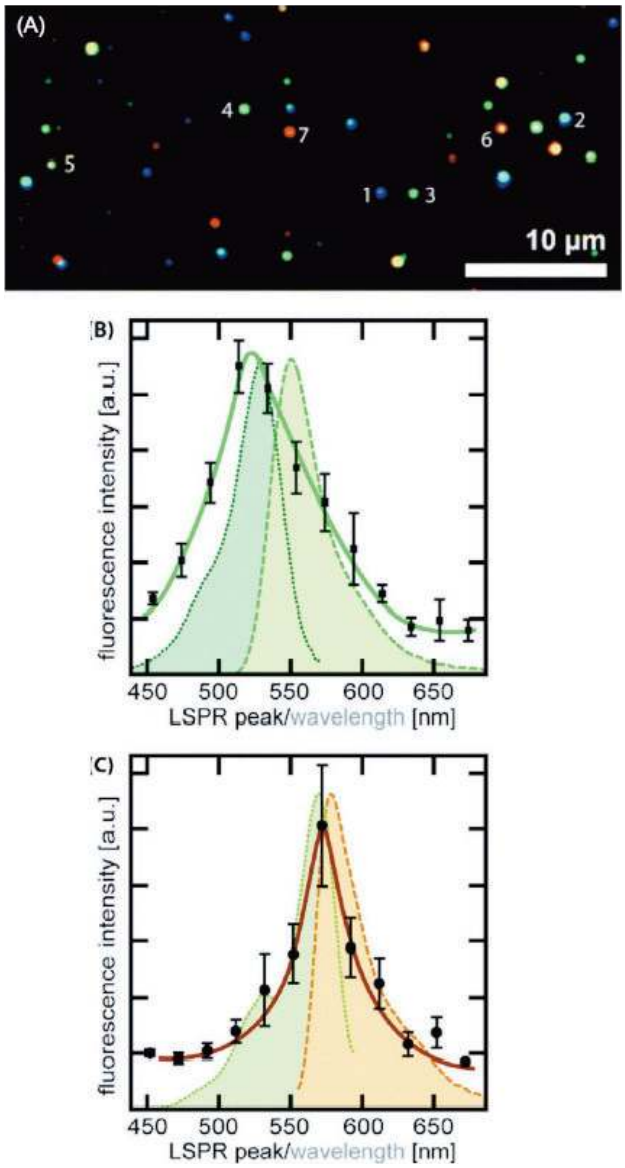

Figure 12 (online color at: www.lpr-journal.org) (a) Darkfield-microscope image of several silver nanoparticles of different shapes. (b, c) Average fluorescence intensity (points) for (b) Alexa Fluor 532 and (c) Rhodamine Red dye molecules bound to individual metal NPs, as a function of the localized surface plasmon resonance (LSPR) frequency in the NPs. Also shown are the excitation spectra (dotted lines) and emission spectra (dashed lines) for the dyes. Reprinted with permission from [139], Copyright (2007) by the American Chemical Society.

have investigated the coupling of one gold NP to one dye molecule [141, 142]. In these measurements, the gold particle is attached to the tip of a tapered optical fiber, and an NSOM system is used to approach the NP to an immobilized dye molecule embedded in a thin dielectric layer. This approach allows precise measurements of the emission intensity from a single-oriented molecule as a function of

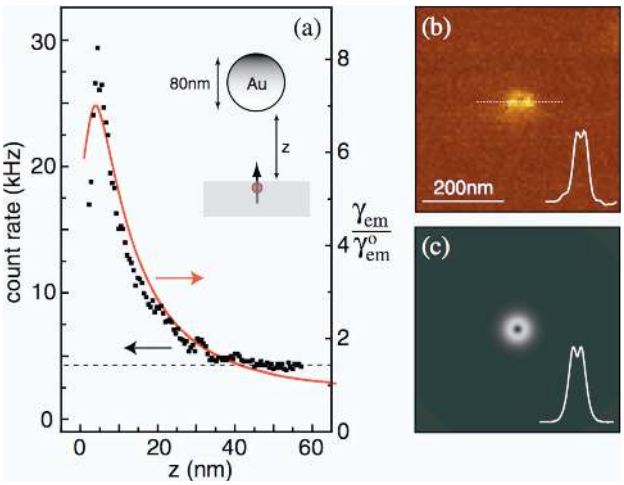

Figure 13 (online color at: www.lpr-journal.org) (a) Detected emission intensity as a function of the distance between a single Nile Blue molecule and an 80-nm gold particle. Points are measured values, the solid line is theory, and the dashed line is the background count rate. (b) Image of fluorescence from the molecule for a vertical separation of approximately 2 nm, as the gold particle is scanned horizontally. (c) Theoretical image. Reprinted figure from [142], Copyright (2006) by the American Physical Society.

its separation from the gold NP, as shown in Fig. 13. Both enhancement and quenching were observed, due to the combined effects of enhanced absorption, increased radiative rate, and non-radiative energy transfer. The results could be compared quantitatively to theory without requiring any adjustable parameters. These measurements thus represent an important step towards the quantitative understanding of the coupling between emitters and metal NPs.

4. Understanding NP plasmonics

As well as the ability to fabricate and measure well-characterized nanostructures, progress in plasmonics requires the development of an accurate theoretical understanding of the optical response of the structures. Two principle challenges in developing this understanding are (1) having an accurate description for the response of the electron plasma in the material that makes up the NP, and (2) determining the effect of the particle geometry on the electromagnetic fields. The most common approach to the first issue is the classical dielectric formalism, where the material linear response is described by a local bulk dielectric function $\varepsilon(\omega)$. Using this dielectric function, Poisson's equation (in the electrostatic limit) or Maxwell's equations are solved for the electromagnetic fields, with the geometry of the nanostructure setting the boundary conditions. In the next sections, we discuss the methods used to solve this boundary-value problem and review results that illustrate the effects of NP geometry and coupling on plasmonic response.

© 2008 by WILEY-VCH Verlag GmbH & Co. KGaA, Weinheim

4.1. Linear response: basics

The first theoretical studies, early in the twentieth century, to address light scattering by NPs were based on analytical solutions of Maxwell's equations for simple geometries, such as spheres [143] and ellipsoids [144]. In the simplest model used for the dielectric response, the response of the free-electron plasma is characterized by a harmonic oscillator. The resulting dielectric function is given by the Drude formula, $\varepsilon(\omega) = 1 - \omega_p^2/(\omega(\omega + i\gamma))$, where γ is the frequency dependent damping and ω_p is the bulk metal plasma frequency, which depends on the metal electron density, n, the electron charge, e, and the electron mass, m_e, through $\omega_p^2 = 4\pi ne^2/m_e$. For spheres, the solutions, known as Mie resonances, are shown in Fig. 14(a) as a function of radius, a. The lowest mode is dipolar (l =1), and is often referred to as the spherical plasmon. For small particles ($a \ll c/\omega_p$), the energy of this mode is $\hbar\omega = \hbar\omega_p/\sqrt{3}$. This mode redshifts as the particle size increases, due to retardation effects. This is the mode typically excited by linearly polarized light and is responsible for the dominant feature in the optical spectra of colloids. This is illustrated in Fig. 14(b), which shows typical absorption, scattering and extinction optical spectra for a 10 nm particle in vacuum. As well as the dipole mode, higher-order, multipolar modes ($l = 2, 3, \ldots$) can also be excited [145]. The energy of these modes tends toward the plasmon energy of the planar surface, $\hbar\omega_p/\sqrt{2}$, as $l \to \infty$, as shown in Fig. 14(a). Similar spectra are obtained for geometries which depart slightly from spherical shape, such as spheroids [96] and disks [146].

Analytical and semi-analytical solutions have been obtained for the surface plasmon modes of a variety of structures with increasing structural complexity, including slabs [147], cylinders [148, 149], cubes [150], edges [151], hemispheres [152], coupled spheres [153, 154], and NP arrays [155, 156]. However, to understand the optical response of more complex nanostructures, it is necessary to use rigorous computational approaches capable of handling arbitrary geometries. Quantitative theories based on empirical dielectric response functions, rather than simple Drude models, also motivate the use of computational approaches. Among the numerical methods most commonly used are the finite difference time domain (FDTD) method [157], the discrete dipole approximation (DDA) [158, 159], Greens function approaches similar in spirit to the DDA [160], the multiple multipole (MMP) method [161], multiple scattering techniques, transfer matrix approaches [162], plane wave expansions [163], and boundary element methods (BEM) [164].

All of these approaches have advantages and disadvantages. Plane wave expansions and transfer matrix approaches work well for arrays of NPs, but are more difficult to apply for finite geometries. FDTD calculations involve the discretization of Maxwell's equations on a grid that encompasses the NPs to be studied and the region where fields are to be determined. Fields are found by propagating Maxwell's equations forward in time. Similar approaches can be applied in the frequency domain. It is straightforward to apply this method to structures with arbitrary geometries. However, it is a volume approach, scaling rapidly with the size of the system to be studied, including both the particles and the regions where fields are determined. Moreover, sys-

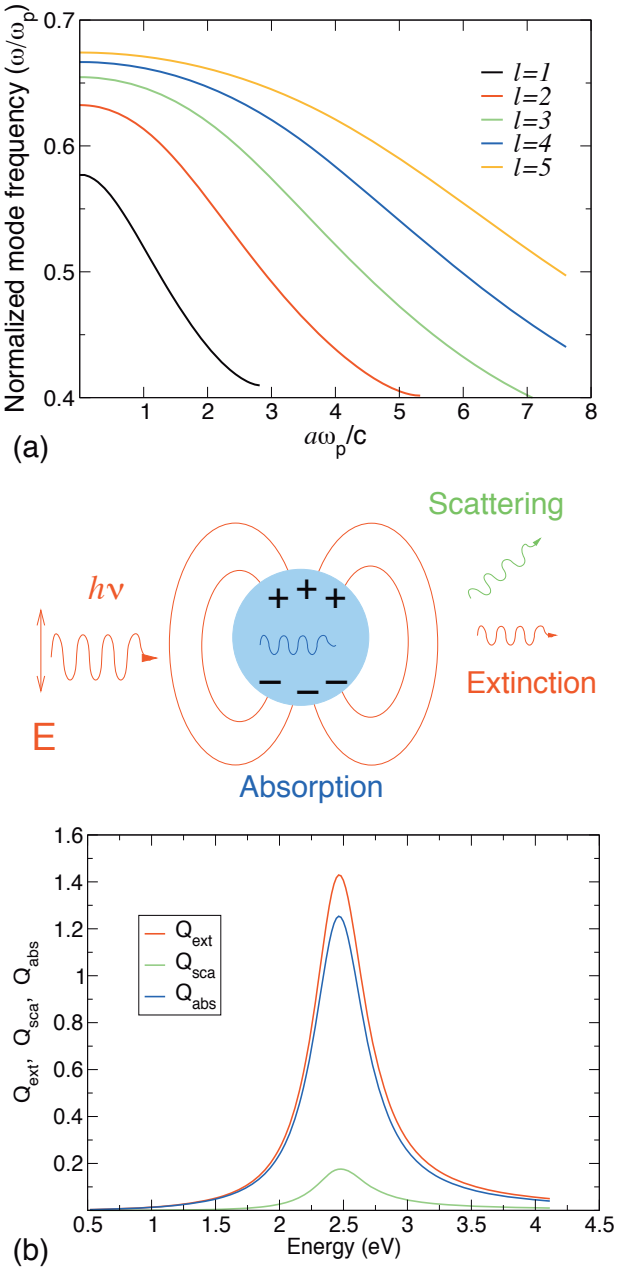

Figure 14 (online color at: www.lpr-journal.org) (a) Modes of a spherical metal NP as a function of the particle radius a. Dipolar ($l = 1$), quadrupolar ($l = 2$), and higher-order modes are plotted. Mode frequencies are normalized by the bulk plasmon frequency ω_p. (b) Scattering, absorption and extinction coefficients (cross sections normalized by the particle geometrical area) for a spherical metal NP of radius $a = 10$ nm, and schematic of the scattering geometry.

© 2008 by WILEY-VCH Verlag GmbH & Co. KGaA, Weinheim

tems with multiple length scales are difficult to study with the uniform grids typically employed. In addition, FDTD can have problems treating media with high dielectric contrast, such as metals. Nonetheless, the FDTD method is one of the most widely used and successful approaches, and can be augmented with accurate representations of the metal dielectric response.

In the DDA, the structures are represented by a grid of discrete, mutually interacting dipoles, whose response is solved in order to determine the optical properties of the structures. The DDA is intuitively compelling and, like the FDTD method, straightforward to apply to arbitrary structures. Although the DDA is also a volume approach, only the structures must be discretized, and fields outside the structures are determined directly from the fields generated by the dipoles. Multiple length scales, though, can still be a problem, with accurate calculations of fields near a nanostructured surface requiring high densities of dipoles.

The MMP and BEM both scale with the area of the system surfaces and can, in principle, be computationally more efficient than volume approaches. In the MMP, fields are represented via multipolar expansions. Different spatial regions are described by different expansions. The multipole coefficients are determined by solving the boundary conditions for Maxwell's equations at a grid of points on the surfaces separating different regions. This approach can best be applied when these surfaces are easily defined. For symmetrical structures, the placement and the form of the multipole expansions are clear, and a limited number of multipoles can describe an entire system. For more complicated structures, the number, placement and form of the multipoles are less obvious. There may be many reasonable choices, making the choice arbitrary and more difficult to reliably control.

In the boundary element method, the boundary conditions for Maxwell's equations are set up at a grid of points on the surfaces between different regions and are then solved in terms of the effective charges and currents on those surfaces. The resulting fields can subsequently be found throughout space. The BEM easily handles variable grids, which allows, for example, surface regions where fields are highly localized to be treated with a high-density grid, without expending the same computational effort elsewhere where requirements are less demanding. Like the MMP, the BEM is well suited for problems where the surfaces are smooth and can be easily defined. It is more difficult to use for complex surfaces or surfaces with sharp contours and edges.

4.2. Nanorods: dependence on size and shape

A principal goal of modeling the optical properties of metal NPs is to develop a general understanding of how plasmon resonances are determined by NP size and shape. Gold nanorods provide a good model system for developing this understanding, because they have been studied theoretically in detail [165–178], and because their relatively simple

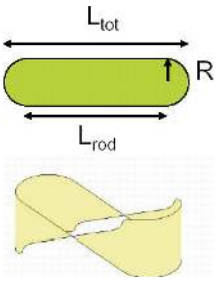

Figure 15 (online color at: www.lpr-journal.org) Top: schematic and dimensions of a cylindrical nanorod with hemispherical ends. Bottom: surface charge density along the edge of the rod for a dipole resonance.

geometry can be readily manipulated to reveal rich behavior. Moreover, nanorod plasmon resonances can be tuned over a wide range by changing the nanorod size, shape and composition, providing large local-field enhancements and intense far-field scattering.

A simple model of the nanorod, illustrated in Fig. 15, as a cylindrical rod of length $L_{\rm rod}$, radius R, with hemispherical end caps and total length $L_{\rm tot} = L_{\rm rod} + 2R$ provides a good approximation for the typical geometry of real particles. The near- and far-field optical response for such rods of different lengths, calculated exactly, including retardation, by means of the boundary element method [165, 179], are shown in Fig. 16 [165]. The far-field

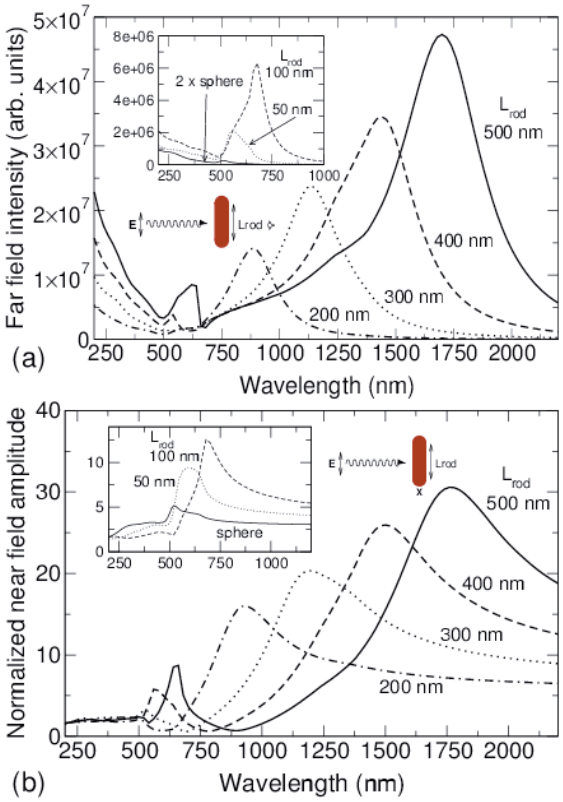

Figure 16 (online color at: www.lpr-journal.org) (a) Far-field scattering intensity as a function of wavelength for a plane wave incident on an Au nanorod of radius $R = 40$ nm, as depicted in the schematic. (b) Normalized near-field amplitude 1 nm from the nanorod end. From [165].

© 2008 by WILEY-VCH Verlag GmbH & Co. KGaA, Weinheim

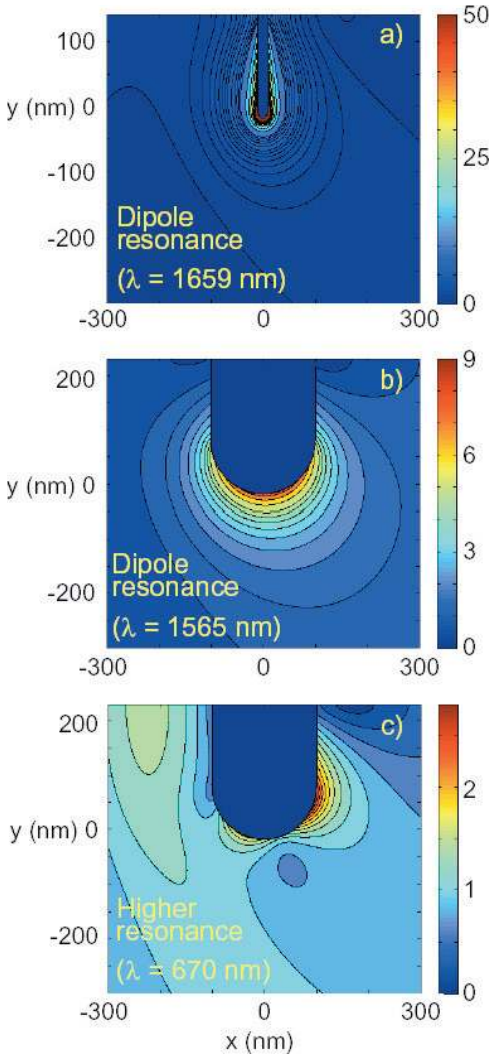

Figure 17 (online color at: www.lpr-journal.org) Electric-field magnitudes for dipolar resonances of gold nanorods with lengths $L_{\rm rod} = 300$ nm and radii (a) $R = 10$ nm and (b) $R = 100$ nm. A higher resonance for $R = 100$ nm is shown in (c).

response below 500 nm is a bulk response and does not occur in the near field. The longest-wavelength peak in the response corresponds to the dipole resonance. Fig. 15 shows a typical surface charge density for this mode [165]. The charge oscillation is cut off at the rod ends and is less than half a wavelength long. Typical near-field distributions for dipolar resonances are shown in Fig. 17. The normalized near-field can be significantly enhanced near the ends of the nanorods. Resonance peaks at shorter wavelengths are assigned to higher-order resonances. All of these longitudinal resonances redshift with increasing rod length, because the restoring force due to the charge separation weakens as the charge is separated over longer distances. Light polarized perpendicular to the rod axis, by contrast, excites transverse resonances, which blueshift slightly with increasing rod length.

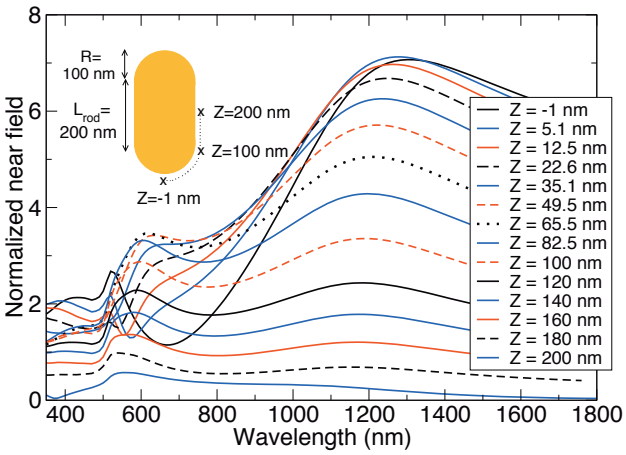

Figure 18 (online color at: www.lpr-journal.org) Position dependence of the near-field response of a gold nanorod with length $L_{\rm rod} = 200$ nm and radius $R = 100$ nm. The positions shown are 1 nm from the rod surface, along the dashed line shown in the inset, labeled by their distance Z along the rod axis from the end. $Z = 200$ nm corresponds to the point at the middle of the rod. $Z = -1$ nm corresponds to the point 1 nm outside the end of the rod. The incident field is polarized along the axis of the rod.

The near-field resonance wavelength depends strongly on the location along the rod where it is measured. A blueshift of the resonance is observed as the measurement position is moved along the rod from the end to the center, while remaining a fixed distance away from the surface, as shown in Fig. 18. Near the center of the rod, in fact, the dipolar resonance disappears. This variation of the resonance along the rod axis is of great importance for any application that exploits the plasmon resonance to modify the response of attached molecules or other nanostructures.

The peak wavelengths for the dipolar resonance, as extracted from the calculated spectra for the far field and the normalized near-field response, increase approximately linearly with increasing $L_{\rm tot}$, except when the longitudinal dimension $L_{\rm tot}$ is comparable to the lateral dimension $2R$ and end effects are dominant. For small R, dipole resonance wavelengths extracted from the far field and near field response are nearly identical. As R increases, the near-field resonance becomes noticeably redshifted from the far-field resonances. For example, for $R = 100$ nm, the redshift is about 200 nm, comparable to the resonance half-width. This shift is a signature of the onset of retardation effects, which become important for rod diameters on the order of one fifth of a wavelength.

As the nanorod length increases, the higher-order resonances appear, initially having wavelengths near the resonance for a spherical nanoparticle, and then redshifting linearly with $L_{\rm tot}$ [165]. For smaller R, the shorter-wavelength resonances that appear first are the higher-order longitudinal resonances. For thicker nanorods, on the other hand, the first higher-order resonance that appears can be a transverse mode with strong far-field response and weak

© 2008 by WILEY-VCH Verlag GmbH & Co. KGaA, Weinheim

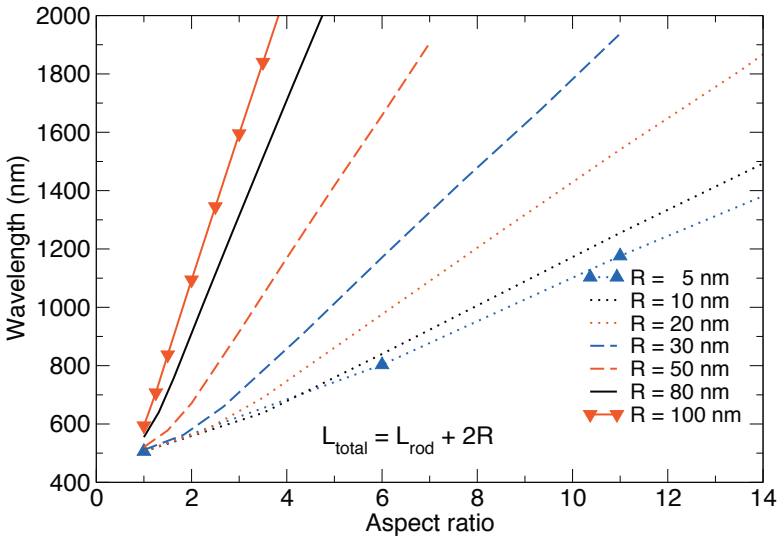

Figure 19 (online color at: www.lpr-journal.org) The dependence of the dipole resonance wavelength on aspect ratio $L_{\rm tot}/(2R)$ for different radii R. The resonance wavelength is extracted from the far-field scattering spectrum.

near-field response at the rod end, as illustrated in Fig. 17. That a transverse mode can be driven by a longitudinal polarization is another signature of the onset of retardation effects: the surface charges on opposite sides of the nanorod are driven by local incident fields with different phases.

Recently, the analogy between nanorods, acting as optical-frequency nanoantennas, and traditional microwave and radio-wave antennas has been brought out and explored [12, 13, 165, 180–183]. Linear scaling of the plasmon resonance wavelength $\lambda_{\rm res}$ with total nanorod length $L_{\rm tot}$ emphasizes this analogy. The dipolar mode of such nanoantennas is often referred to as the $\lambda/2$ mode, with the expectation that the resonance should occur when $L_{\rm tot}$ is a half wavelength, as happens for traditional long-wavelength antennas made from nearly perfect conductors. While such an assignment is tempting, it has not been established, and simulations [165, 182] suggest that it is not the case. Rather, the results of boundary-element calculations indicate that the linear dependence of the dipole resonance on $L_{\rm tot}$ varies substantially with R. For a half-wavelength antenna made from a perfect conductor, the resonance wavelength and rod length should be related according to $L_{\rm tot} = L_0 + S\lambda_{\rm res}$, with a slope $S = 1/2$. For small R, nanoantennas have $S \sim 0.2$ [179], indicating that much less than a half-wavelength of surface charge oscillation fits on the nanorod at resonance (as seen in Fig. 15). This deviation from the perfect-conductor case is partially due to the finite skin depth of gold, which is on the order of 20 nm to 30 nm for the wavelengths considered [182]. In addition, the sharp ends of the rods inhibit full charge build-up, suppressing half-wavelength charge oscillations that have peak charge density at the rod ends. As R increases, the slope S monotonically increases, converging to 0.4. This means that nanoantennas remain far away from a $\lambda/2$ antennas, even for micrometer-size structures.

It is well known that, in the quasistatic limit, where the light wavelength is much larger than the particle size, the plasmon resonance should be independent of particle size. Because the quasistatic model is simple but intuitively compelling, much of the theoretical work has highlighted the dependence of the plasmon resonance on aspect ratio, ignoring any explicit dependence on nanorod length or radius. A full mapping of the plasmon dipole resonances in nanorods from full electromagnetic calculations, including retardation, provides a stringent test for the this approach. The dependence on aspect ratio is shown in Fig. 19 for different R [179]. In the quasistatic limit, the plasmon resonance should be independent of R, and all curves should be identical. Surprisingly, there is no such region, except for the very smallest, nearly spherical NPs. These results show that the requirement that the radius be much less than the wavelength is very stringent, and, outside of this highly restricted range, the quasistatic approximation is limited.

4.3. Coupled plasmons

The optical response of complex nanostructures can often be understood in terms of the coupling of plasmons in simpler components that make up the structure. For example, extinction measurements have shown that the plasmon resonance of gold nanorings, fabricated using lithographic techniques and latex sphere templates, is strongly redshifted as compared to the response of a disk with the same size [61]. Full electromagnetic calculations accurately describe the positions of the plasmon resonances, their widths, and the large redshift of the nanoring response as the ring thickness decreases. Most importantly, the calculations show that this redshift is due to increased coupling between plasmons on the inner and outer edges of the nanorings (see Fig. 20).

The response of even more complex NPs, such as the gold nanostars [54, 184] shown in Fig. 21, can also be accurately modeled. The interpretation of nanostar spectra requires a sophisticated calculational method, such as the FDTD method. The modes of the tips and of the core of the nanostar can be resonantly excited, depending on the polar-

© 2008 by WILEY-VCH Verlag GmbH & Co. KGaA, Weinheim

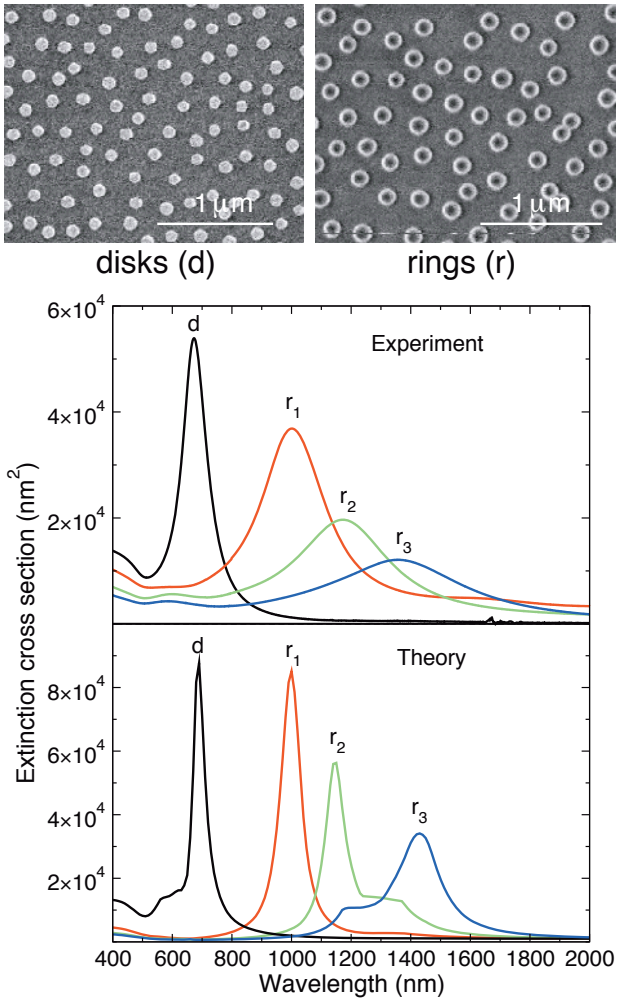

Figure 20 (online color at: www.lpr-journal.org) Measured extinction spectra for gold nanodisks and gold nanorings and the corresponding calculated spectra. Micrographs of the disks and rings are also shown. The disk and ring diameters are 120 nm. The thickness of the ring walls are 14 nm, 10 nm, and 9 nm for r_1, r_2, and r_3, respectively. From [61].

ization of the incoming light. The coupling between the tip modes and the core modes produce wavelength shifts, as depicted in Fig. 21(c).

For nanorings and nanostars, the coupling is between different plasmon modes on the same particle. Even more significant effects can be seen when two separate metal NPs are brought together and their individual plasmons couple. The wavelength shift resulting from this interparticle coupling depends sensitively on the particle separation, providing a clear signature useful for sensing applications. While near-fields around single NPs can be strongly enhanced, the near-fields in the gaps between NPs can be enhanced by several additional orders of magnitude due to the interaction between the particles. Such "hot spots" are key to many applications in field-enhanced microscopy, spectroscopy, sensing, and manipulation [10, 185, 186].

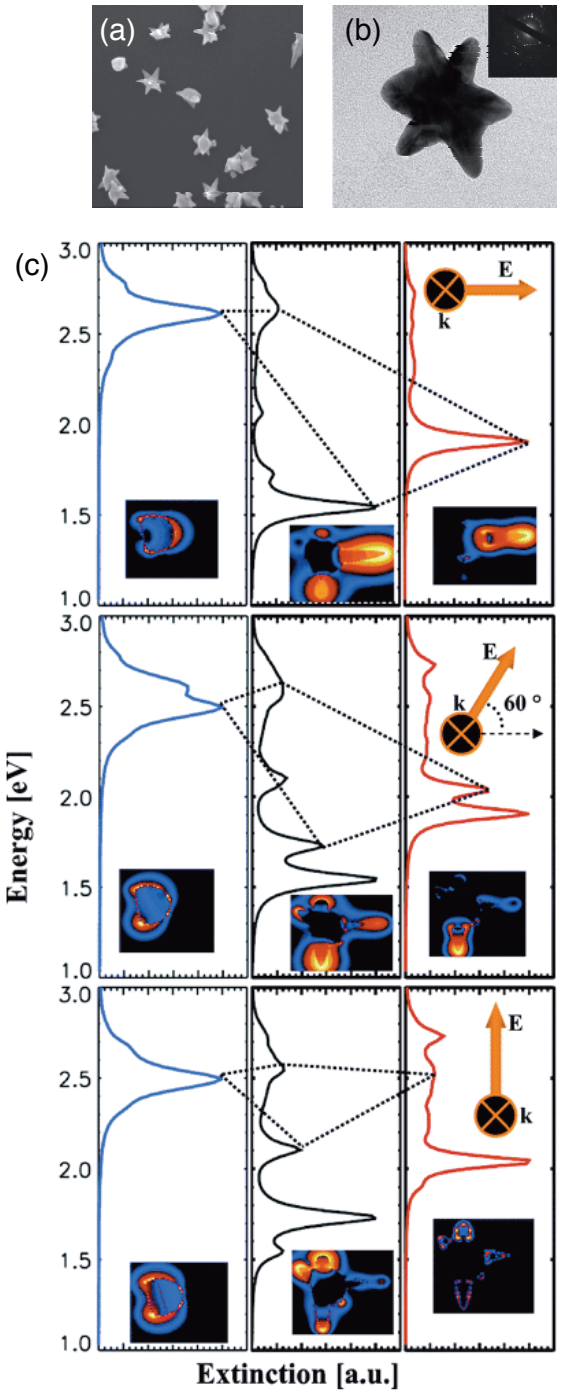

Figure 21 (online color at: www.lpr-journal.org) (a) Micrographs of gold nanostars. (b) Geometry for in the finite-difference time-domain calculations used to model the nanostar. (c) Calculated extinction spectra for different incident polarizations of light together with the near-field patterns of the modes associated with the different peaks. Panels on the left correspond to the isolated core, panels to the right correspond to the isolated tips, and panels in the center to the whole nanostar. Dashed lines connect core and tip resonances to the coupled resonances in the nanostar. Reprinted with permission from [54] and [184], Copyright (2006) and (2007) American Chemical Society.

© 2008 by WILEY-VCH Verlag GmbH & Co. KGaA, Weinheim

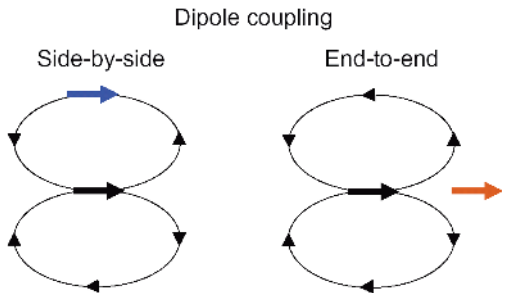

Figure 22 (online color at: www.lpr-journal.org) Schematic of dipole-dipole coupling. The field lines of the black dipole are indicated.

The concept of plasmon hybridization [187, 188] provides a simple way to understand coupling between plasmons. In much the same way that atomic orbitals hybridize to form bonding and antibonding orbitals in molecules, plasmons in different particles can couple in phase or out of phase, with the strength of the coupling determining the induced resonance shift. The effect of plasmon hybridization can be seen by considering two coupled dipoles, as illustrated in Fig. 22. In the optically active, hybridized mode of a pair, the two dipoles oscillate in phase to give the pair a net dipole. Hybridization can redshift or blueshift the resonance, depending on the dipole orientation. When the dipoles are coupled end-to-end, the field generated by one dipole (the black dipole in the figure) at the second dipole is in phase with the polarization of the first dipole. Because these dipoles behave as driven harmonic oscillators, the second dipole responds in phase to the driving field, at frequencies below the single-dipole resonance. As a consequence, the optically active, hybridized mode of the pair is redshifted from the single-dipole resonance frequency. When the dipoles are coupled side-by-side, the field generated by the black dipole at the second dipole is out of phase with the polarization of the first dipole. The second dipole responds out of phase to the driving field, at frequencies blueshifted from the single-dipole resonance.

Plasmon hybridization provides an intuitive picture for plasmon coupling, particularly in weakly coupled structures. However, in strongly coupled, closely spaced particles, the individual particle plasmons can be significantly distorted, due to mixing of other modes into the hybridized pair. To fully understand plasmon coupling in such cases, detailed calculations are necessary. Fig. 23 shows the calculated dependence of the dipolar response on the separation between two identical gold rods [165]. Several regimes with clearly different behavior are apparent and have been observed experimentally [146]. For gaps larger than $\lambda/4$, the dipole response of the coupled pair oscillates about the result expected for two noninteracting rods, due to far-field interference effects. For gaps less than $\lambda/4$, the resonance wavelength redshifts, as expected for plasmon hybridization. However, the strong coupling localizes charge near the gap, enhancing the field in the gap and inhibiting the charge oscillation. The separation of dipole charge inside each rod

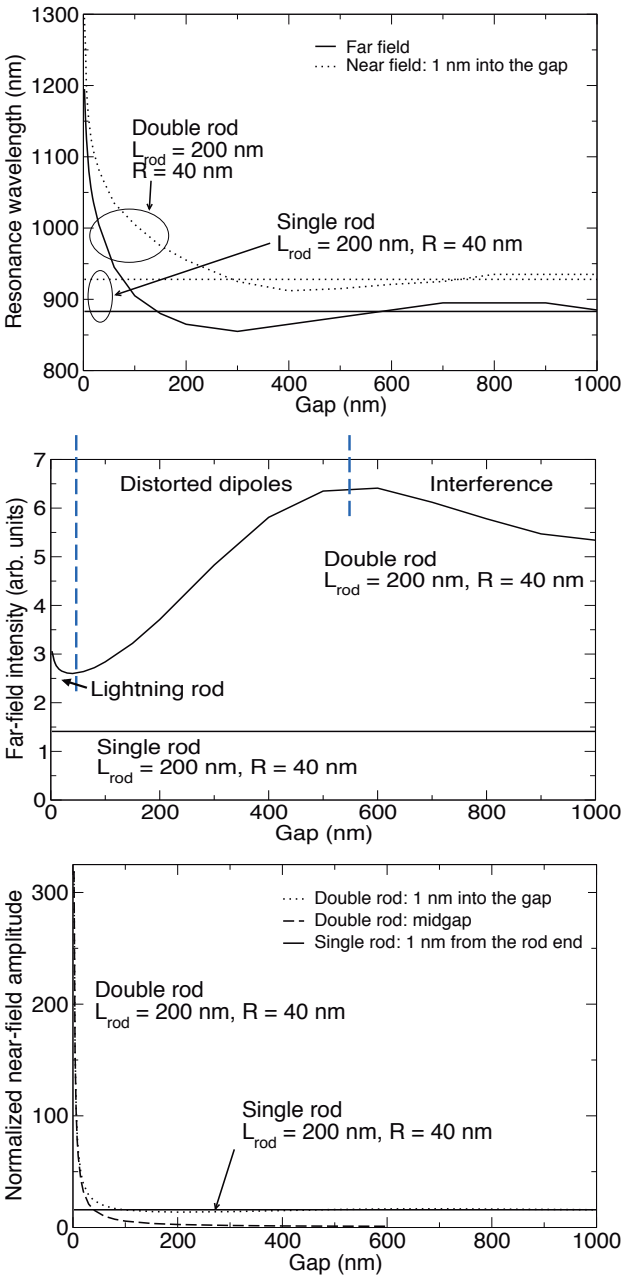

Figure 23 Far-field and near-field response of a pair of identical Au nanorods, coupled end-to-end, as a function of gap separation, for a plane wave incident with polarization along the rods. The peak wavelength for dipolar response, the far-field intensity at this wavelength and the normalized near-field amplitude at this wavelength are shown. The near field at midgap and the near field 1 nm into the gap from the rod end are shown. Corresponding results for an isolated rod are also indicated. For an isolated rod, the near field 1 nm from the rod end is shown.

is reduced, as shown in Fig. 24, reducing the net dipole moment of the pair, and weakening the far-field scattering. For even smaller separations, more than order-of-magnitude increases in the gap field arise, because of additional charge

© 2008 by WILEY-VCH Verlag GmbH & Co. KGaA, Weinheim

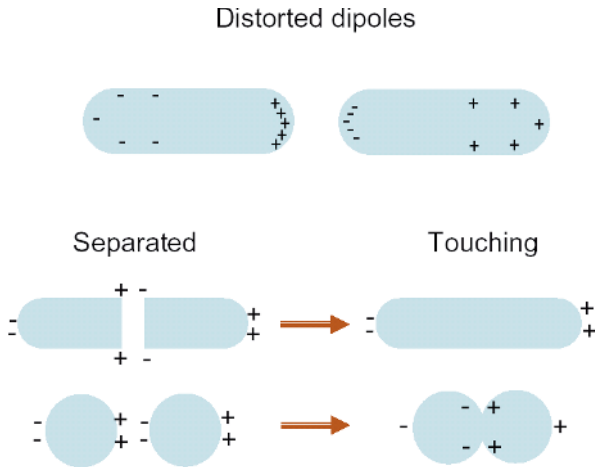

Figure 24 (online color at: www.lpr-journal.org) Distortion of the surface-charge distribution as two metal nanoparticles are brought together, and as they touch. Touching at both a flat surface and a single point of contact are indicated.

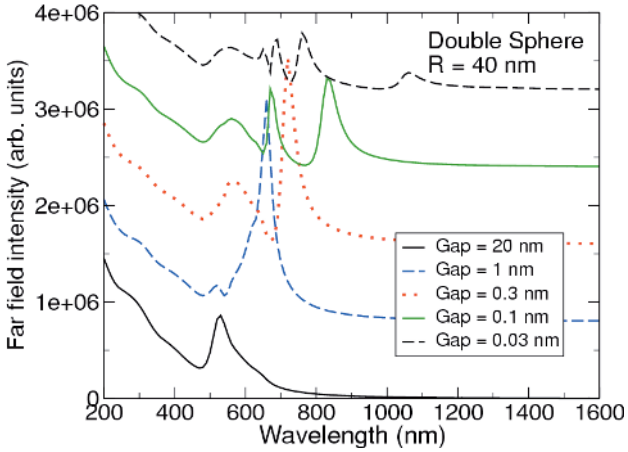

Figure 25 (online color at: www.lpr-journal.org) Spectra of the far-field intensity of a pair of coupled, identical gold nanospheres for different separations between the spheres. The exciting field is polarized along the axis connecting the spheres. The spectra are shifted vertically for clarity.

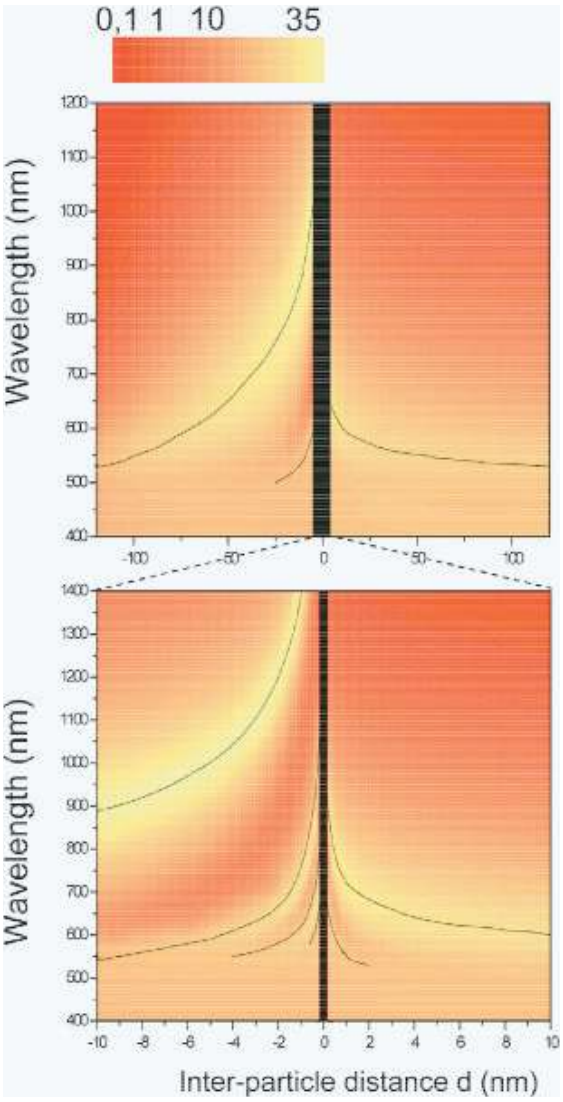

Figure 26 (online color at: www.lpr-journal.org) Scattering cross-section for two gold spheres with radius $R = 60$ nm, as a function of the gap d between their surfaces and the light wavelength, for an incoming field polarized along the axis joining the spheres. Negative values of d correspond to overlapping spheres. The cross section is normalized to that of a single particle. Solid curves show the cross-section maxima. From [189].

localization at the gap, known as the lightning rod effect. The far-field intensity then increases with decreasing gap, as is apparent in both Fig. 23 and Fig. 25.

For gaps smaller than a nanometer [189], the dipole resonance continues to redshift, but the far-field dipole scattering saturates and is then suppressed, as shown in Fig. 25. The charge localization at the gap becomes so large that the dipole mode cannot support additional charge localization, and charge oscillation along the rods is inhibited. At the same time, higher order modes are excited to support the charge localization. However, they also saturate in turn as the gap is decreased.

When the NPs touch and then overlap, additional extreme distortion of the dipole charge can occur. When two NPs touch at a flat surface, the charge at the gap is neutralized, as shown schematically in Fig. 24. The dipole response blueshifts because higher order particle-plasmon modes must be mixed to allow the charge neutralization. However, as shown in Fig. 26, when the the NPs touch at a single point of contact, there is an additional redshift in the dipolar response [189], as has been seen experimentally [146]. The charge at the gap is drastically reorganized but not neutralized: a large net charge builds up on each particle, with most of the charge still localized near the gap, as in Fig. 24. This large charge buildup cannot come from particle-plasmon hybridization or by mixing in higher order

© 2008 by WILEY-VCH Verlag GmbH & Co. KGaA, Weinheim

particle modes, because all such modes are charge neutral on each particle. Rather, the large charge buildup comes from mixing modes, unphysical for single particles, that have net charge on each NP [165].

All the results discussed in this section have been obtained with a local, frequency-dependent dielectric response. Although non-local effects are typically negligible for coupled NPs separated by several tens of nanometers, they may strongly modify the response for much smaller separations, cutting off the singular response when the particles touch [190]. Quantum-mechanical charge tunneling between closely spaced particles further complicates the non-local response. A full quantum-mechanical, self-consistent treatment will be needed to properly model these extreme cases [191, 192].

5. Prospects

In this review, we have discussed the tools and techniques needed to fabricate, characterize, and understand metal-NP plasmonics. The tools now exist to fabricate a wide variety of NP sizes and shapes. Both lithography-based top-down and chemistry-based bottom-up approaches are available. Complex assemblies of metal NPs and hybrid assemblies of metal NPs attached to molecules and to quantum dots can also be made. However, precise control of the particle positioning in these assemblies has not been yet achieved, so the fabrication of well-defined assemblies remains an unsolved challenge. Characterization of the linear response has advanced to the single particle level, allowing the precise determination of the plasmonic properties of individual particles. The main effort now will be the continued push to improve single-particle imaging methods, improving the signal-to-noise ratio and allowing a clear characterization of single-particle nonlinear response. At the same time, a quantitative understanding of the plasmon resonances in complex NPs is now possible with the use of advanced computational approaches. The dependence of plasmon resonance energy, near-field enhancement and localization, and far-field scattering on particle size, shape, and composition can be determined. This understanding is based mostly on classical theory. Quantum theories of these structures must be developed and exploited to more fully understand the transition from plasmonic response in small particles to molecular response in even smaller particles and coupling of metal particle plasmons to quantum emitters like quantum dots and molecules.

As a consequence of these advances, metal-NP plasmonics is poised to have significant impact on a variety of rapidly developing technologies that demand tunability and nanoscale field localization. Applications currently being developed include nanoscale optical and infrared sensing, microscopy, and spectroscopy, in which the metal NPs effectively act as nanoantennas to enhance signal emission. Conversely, metal NPs can act as nanoantennas to collect and localize energy input. Critical uses in medicine, for example to locally and selectively heat and kill cancerous tumors, are already being developed. Nanoscale optical communication along pathways defined by assemblies of coupled NPs, is also being explored as one approach to push electronic and optical technologies down to the nanoscale. Recent experiments even suggest that quantum information could be launched into and passed through assemblies of plasmonic structures. Such developments could push plasmonics into the exotic realm of quantum science.

Acknowledgements We thank M. Liu for his valuable assistance. Work at the Center for Nanoscale Materials was supported by the U. S. Department of Energy, Office of Science, Office of Basic Energy Sciences, under Contract No. DE-AC02-06CH11357.

Matthew Pelton, born in 1975, studied Engineering Science at the University of Toronto. He achieved his Ph. D. in Applied Physics at Stanford University on single quantum dots coupled to microcavities. After research positions at the Royal Institute of Technology (Stockholm, Sweden) and at the University of Chicago, he started his current position at the Center for Nanoscale Materials at Argonne National Laboratory.

Javier Aizpurua, born in 1971, studied physics at the University of Zaragoza (Spain). He achieved his Ph. D. at the University of the Basque Country on the theory of plasmon excitation by fast electron beams. After research positions at Chalmers University of Technology (Sweden) and NIST (USA), he worked at the Donostia International Physics Center (Spain). He currently holds a position as senior researcher of the Spanish Council for Scientific Research (CSIC) at the Materials Physics Center in San Sebastián, doing theoretical research on nano-optics.

Garnett Bryant studied physics at the University of Kentucky. He achieved his Ph. D. at Indiana University in theoretical condensed matter physics. After research positions at Washington State University, the National Bureau of Standards, McDonnell Research Labs and the Army Research Laboratory, he has worked at the National Institute of Standards and Technology (NIST). He currently is group leader of the Quantum Processes and Metrology Group at NIST, and a fellow of the Joint Quantum Institute of NIST/University of Maryland, doing theoretical research on nanosystems, nanooptics and quantum science.

© 2008 by WILEY-VCH Verlag GmbH & Co. KGaA, Weinheim

References

[1] H. A. Atwater, Sci. Am. (USA) **296**, 56 (2007).
[2] S. Lal, S. Link, and N. J. Halas, Nature Photonics **1**, 641 (2007).
[3] D. Bohm and D. Pines, Phys. Rev. **82**, 625 (1951).
[4] R. H. Ritchie, Phys. Rev. **106**, 874 (1957).
[5] U. Kreibig and M. Vollmer, Optical Properties of Metal Clusters (Springer-Verlag, Berlin, 1995).
[6] C. F. Bohren and D. R. Huffman, Absorption and Scattering of Light by Small Particles (Wiley, New York, 1983).
[7] M. Durach, A. Rusina, M. I. Stockman, and K. Nelson, Nano Lett. **7**, 3145 (2007).
[8] S. M. Nie and S. R. Emory, Science **275**, 1102 (1997).
[9] K. Kneipp, Y. Wang, H. Kneipp, L. T. Perelman, I. Itzkan, R. R. Dasari, and M. S. Feld, Phys. Rev. Lett. **78**, 1667 (1997).
[10] H. Xu, E. J. Bjerneld, M. Käll, and L. Börjesson, Phys. Rev. Lett. **83**, 4357 (1999).
[11] H. Xu, J. Aizpurua, M. Käll, and P. Apell, Phys. Rev. E **62**, 4318 (2000).
[12] F. Neubrech, T. Kolb, R. Lovrincic, G. Fahsold, A. Pucci, J. Aizpurua, T. W. Cornelius, M. E. Toimil-Molares, R. Neumann, and S. Karim, Appl. Phys. Lett. **89**, 253104 (2006).
[13] T. H. Taminiau, R. J. Moerland, F. B. Segerink, L. Kuipers, and N. F. van Hulst, Nano Lett. **7**, 28 (2007).
[14] F. Tam, G. P. Goodrich, B. R. Johnson, and N. J. Halas, Nano Lett. **7**, 496 (2007).
[15] R. Hillenbrand, F. J. Keilmann, P. Hanarp, D. S. Sutherland, and J. Aizpurua, Appl. Phys. Lett. **83**, 368 (2003).
[16] T. Kalkbrenner, U. Håkanson, A. Schädle, S. Burger, C. Henkel, and V. Sandoghdar, Phys. Rev. Lett. **95**, 200801 (2005).
[17] L. Novotny and B. Hecht, Principles of Nano-optics (Cambridge University Press, Cambridge, 2006).
[18] M. L. Brongersma, J. W. Hartman, and H. A. Atwater, Phys. Rev. B **62**, R16356 (2000).
[19] S. A. Maier, M. L. Brongersma, P. G. Kik, S. Meltzer, A. A. G. Requicha, and H. A. Atwater, Adv. Mater. **13**, 1501 (2001).
[20] S. A. Maier, P. G. Kik, H. A. Atwater, S. Meltzer, E. Harel, B. E. Koel, and A. A. G. Requicha, Nature Mater. **2**, 229 (2003).
[21] C. Girard and R. Quidant, Opt. Express **12**, 6141 (2004).
[22] L. A. Sweatlock, S. A. Maier, H. A. Atwater, J. J. Penninkhof, and A. Polman, Phys. Rev. B **71**, 235408 (2005).
[23] S. Bozhevolnyi, V. Volkov, E. Devaux, and T. Ebbesen, Phys. Rev. Lett. **95**, 046802 (2005).
[24] J. B. Pendry, Phys. Rev. Lett. **85**, 3966 (2000).
[25] V. M. Shalaev, Nature Photonics **1**, 41 (2007).
[26] W. A. Murray and W. L. Barnes, Adv. Mater. **19**, 3771 (2007).
[27] N. Fang, H. Lee, C. Sun, and X. Zhang, Science **308**, 534 (2005).
[28] A. Yildiz, J. N. Forkey, S. A. McKinney, T. Ha, Y. E. Goldman, and P. R. Selvin, Science **300**, 2061 (2003).
[29] J. R. Lakowicz, Anal. Biochem. **337**, 171 (2005).
[30] L. R. Hirsch, R. J. Stafford, J. A. Bankson, S. Sershen, B. Rivera, R. E. Price, J. D. Hazle, N. J. Halas, and J. West, Proc. Natl. Acad. Sci. USA **100**, 13549 (2003).
[31] A. G. Skirtach, C. Dejugnat, D. Braun, A. S. Susha, A. L. Rogach, W. J. Parak, H. Möhwald, and G. B. Sukhorukov, Nano Lett. **5**, 1371 (2005).
[32] P. Rai-Choudhury (ed.), Handbook of Microlithography, Micromachining, and Microfabrication (SPIE Publications, Bellingham, Washington, 1997).
[33] C. L. Haynes, A. D. McFarland, L. L. Zhao, R. P. van Duyne, G. C. Schatz, L. Gunnarsson, J. Prikulis, B. Kasemo, and M. Käll, Nano Lett. **107**, 7337 (2003).
[34] W. Rechberger, A. Hohenau, A. Leitner, J. R. Krenn, B. Lamprecht, and F. R. Aussenegg, Opt. Commun. **220**, 137 (2003).
[35] D. P. Fromm, A. Sundaramurthy, P. J. Schuck, G. Kino, and W. E. Moerner, Nano Lett. **4**, 957 (2004).
[36] A. A. Tseng, J. Micromech. Eng. **14**, R15 (2004).
[37] T. W. Ebbesen, H. J. Lezec, H. F. Ghaemi, T. Thio, and P. A. Wolff, Nature **391**, 667 (1998).
[38] J. Henzie, M. H. Lee, and T. W. Odom, Nature Nanotech. **2**, 549 (2007).
[39] J. Henzie, E. S. Kwak, and T. W. Odom, Nano Lett. **5**, 1199 (2005).
[40] M. Faraday, Philos. Trans. R. Soc. London **147**, 145 (1857).
[41] J. Turkevich, P. C. Stevenson, and J. Hilier, Disc. Farad. Soc. **11**, 55 (1951).
[42] G. Frens, Nature Phys. Sci. **241**, 20 (1973).
[43] M. Brust, M. Walker, D. Bethell, D. J. Schiffrin, and R. Whyman, J. Chem. Soc., Chem. Commun. p. 801 (1994).
[44] D. V. Leff, P. C. Ohara, J. R. Heath, and W. M. Gelbart, J. Phys. Chem. **99**, 7036 (1995).
[45] J. M. Petroski, Z. L. Wang, T. C. Green, and M. A. El-Sayed, J. Phys. Chem. B **102**, 3316 (1998).
[46] Y. Sun and Y. Xia, Science **298**, 2176 (2002).
[47] Y. Sun, Y. Yin, B. T. Mayers, T. Herricks, and Y. Xia, Chem. Mater. **14**, 4736 (2002).
[48] Y. Sun and Y. Xia, Adv. Mater. **14**, 833 (2002).
[49] N. R. Jana, L. Gearheart, and C. J. Murphy, Adv. Mater. **13**, 1389 (2001).
[50] N. R. Jana, L. Gearheart, and C. J. Murphy, J. Phys. Chem. B **105**, 4065 (2001).
[51] N. R. Jana, L. Gearheart, and C. J. Murphy, Chem. Commun. p. 617 (2001).
[52] B. Nikoobakht and M. A. El-Sayed, Chem. Mater. **15**, 1957 (2003).
[53] M. Liu and P. Guyot-Sionnest, J. Phys. Chem. B **109**, 22192 (2005).
[54] C. L. Nehl, H. Liao, and J. H. Hafner, Nano Lett. **6**, 683 (2006).
[55] J. R. Heath, C. M. Knobler, and D. V. Leff, J. Phys. Chem. B **101**, 189 (1997).
[56] A. Tao, P. Sinsermsuksakul, and P. Yang, Nature Nanotech. **2**, 435 (2007).
[57] X. M. Lin, H. M. Jaeger, C. M. Sorensen, and K. J. Klabunde, J. Phys. Chem. B **105**, 3353 (2001).
[58] T. P. Bigioni, X. M. Lin, T. T. Nguyen, E. I. Corwin, T. A. Witten, and H. M. Jaeger, Nature Mater. **5**, 265 (2006).
[59] J. C. Hulteen and R. P. van Duyne, J. Vac. Sci. Technol. A **13**, 1553 (1995).
[60] U. C. Fischer and H. P. Zingsheim, J. Vac. Sci. Technol. **19**, 881 (1981).

© 2008 by WILEY-VCH Verlag GmbH & Co. KGaA, Weinheim

[61] J. Aizpurua, P. Hanarp, D. S. Sutherland, M. Käll, G. W. Bryant, and F. J. García de Abajo, Phys. Rev. Lett. **90**, 057401 (2003).
[62] Y. Cui, M. T. Björk, J. A. Liddle, C. Sönnichsen, B. Boussert, and A. P. Alivisatos, Nano Lett. **4**, 1093 (2004).
[63] J. A. Liddle, Y. Cui, and A. P. Alivisatos, J. Vac. Sci. Technol. B **22**, 3409 (2004).
[64] K. K. Caswell, J. N. Wilson, U. H. F. Bunz, and C. J. Murphy, J. Am. Chem. Soc. **125**, 13914 (2003).
[65] K. G. Thomas, S. Barazzouk, B. I. Ipe, S. T. S. Joseph, and P. V. Kamat, J. Phys. Chem. B **108**, 13066 (2004).
[66] Z. Nie, D. Fava, E. Kumacheva, S. Zou, G. C. Walker, and M. Rubinstein, Nature Mater. **6**, 609 (2007).
[67] Nobel Lectures in Chemistry 1922–1941 (Elsevier, Amsterdam, 1965).
[68] S. Schultz, D. R. Smith, J. J. Mock, and D. A. Schultz, Proc. Natl. Acad. Sci. USA **97**, 966 (2000).
[69] C. Sönnichsen, T. Franzl, T. Wilk, G. von Plessen, J. Feldmann, O. Wilson, and P. Mulvaney, Phys. Rev. Lett. **88**, 077402 (2002).
[70] J. J. Mock, M. Barbic, D. R. Smith, D. A. Schultz, and S. Schultz, J. Chem. Phys. **116**, 6755 (2002).
[71] C. Sönnichsen, S. Geier, N. E. Hecker, G. von Plessen, J. Feldmann, H. Diltbacher, B. Lamprecht, J. R. Krenn, F. R. Aussenegg, V. Z. H. Chan, J. P. Spatz, and M. Möller, Appl. Phys. Lett. **77**, 2949 (2000).
[72] G. P. Wiederrecht, Eur. Phys. J. Appl. Phys. **28**, 3 (2004).
[73] T. Klar, M. Perner, S. Grosse, G. von Plessen, W. Spirkl, and J. Feldmann, Phys. Rev. Lett. **80**, 4249 (1998).
[74] P. M. Adam, S. Benrezzak, J. L. Bijeon, and P. Royer, J. Appl. Phys. **88**, 6919 (2000).
[75] R. Hillenbrand and F. Keilmann, Phys. Rev. Lett. **85**, 3029 (2000).
[76] M. Liu and P. Guyot-Sionnest, J. Phys. Chem. B **108**, 5882 (2004).
[77] A. Arbouet, D. Christofilos, N. D. Fatti, F. Vallée, J. R. Huntzinger, L. Arnaud, P. Billaud, and M. Broyer, Phys. Rev. Lett. **93**, 127401 (2004).
[78] O. L. Muskens, N. D. Fatti, F. Vallée, J. R. Hutzinger, P. Billaud, and M. Broyer, Appl. Phys. Lett. **88**, 063109 (2006).
[79] A. A. Mikhailovsky, M. A. Petruska, M. I. Stockman, and V. I. Klimov, Opt. Lett. **28**, 1686 (2003).
[80] A. A. Mikhailovsky, M. A. Petruska, K. Li, M. I. Stockman, and V. I. Klimov, Phys. Rev. B **69**, 085401 (2004).
[81] K. Lindfors, T. Kalkbrenner, P. Stoller, and V. Sandoghdar, Phys. Rev. Lett. **93**, 037401 (2004).
[82] P. Stoller, V. Jacobsen, and V. Sandoghdar, Opt. Lett. **31**, 2474 (2006).
[83] D. Boyer, P. Tamarat, A. Maali, B. Lounis, and M. Orrit, Science **297**, 1160 (2002).
[84] S. Berciaud, L. Cognet, G. A. Blab, and B. Lounis, Phys. Rev. Lett. **93**, 257402 (2004).
[85] S. Berciaud, L. Cognet, P. Tamarat, and B. Lounis, Nano Lett. **5**, 515 (2003).
[86] S. Berciaud, D. Lasne, G. A. Blab, L. Cognet, and B. Lounis, Phys. Rev. B **73**, 045424 (2006).
[87] R. Antoine, P. F. Brevet, H. H. Girault, D. Bethell, and D. J. Schiffrin, Chem. Commun. p. 1901 (1997).
[88] B. Lamprecht, A. Leitner, and F. R. Aussenegg, Appl. Phys. B **64**, 269 (1997).
[89] Y. H. Liau, A. N. Unterreiner, Q. Chang, and N. F. Scherer, J. Phys. Chem. B **105**, 2135 (2001).
[90] B. Lamprecht, J. R. Krenn, A. Leitner, and F. R. Aussenegg, Phys. Rev. Lett. **83**, 4421 (1999).
[91] M. Lippitz, M. A. van Dijk, and M. Orrit, Nano Lett. **5**, 799 (2005).
[92] E. J. Heilweil and R. M. Hochstrasser, J. Chem. Phys. **82**, 4762 (1985).
[93] M. L. Bloemer, J. W. Haus, and P. R. Ashley, J. Opt. Soc. Am. B **7**, 790 (1990).
[94] K. Puech, W. Blau, A. Grund, C. Bubeck, and G. Cardenas, Opt. Lett. **20**, 1615 (1995).
[95] T. S. Ahmadi, S. L. Logunov, and M. A. El-Sayed, J. Phys. Chem. **100**, 8053 (1996).
[96] S. Link and M. A. El-Sayed, J. Phys. Chem. B **103**, 8410 (1999).
[97] J. H. Hodak, A. Henglein, and G. V. Hartland, J. Phys. Chem. B **104**, 9954 (2000).
[98] C. Voisin, N. D. Fatti, D. Christofilos, and F. Vallée, J. Phys. Chem. B **105**, 2264 (2001).
[99] S. Link and M. A. El-Sayed, Ann. Rev. Phys. Chem. **54**, 331 (2003).
[100] P. B. Johnson and R. W. Christy, Phys. Rev. B **6**, 4370 (1972).
[101] R. Rosei, F. Antonangeli, and U. M. Grassano, Surf. Sci. **37**, 689 (1973).
[102] R. Rosei, Phys. Rev. B **10**, 474 (1974).
[103] M. Guerrisi, R. Rosei, and P. Winsemius, Phys. Rev. B **12**, 557 (1975).
[104] J. H. Hodak, I. Martini, and G. V. Hartland, J. Phys. Chem. B **102**, 6958 (1998).
[105] S. Link, C. Burda, Z. L. Wang, and M. A. El-Sayed, J. Chem. Phys. **111**, 1255 (1999).
[106] J. H. Hodak, A. Henglein, and G. V. Hartland, J. Chem. Phys. **112**, 5942 (2000).
[107] A. Arbouet, C. Voisin, D. Christofilos, P. Langot, N. D. Fatti, F. Vallée, J. Lermé, G. Celep, E. Cottancin, M. Gaudry, M. Pellarin, M. Broyer, M. Maillard, M. P. Pileni, and M. Treguer, Phys. Rev. Lett. **90**, 177401 (2003).
[108] V. Halté, J. Y. Bigot, B. Palpant, M. Broyer, B. Prével, and A. Pérez, Appl. Phys. Lett. **75**, 3799 (1999).
[109] S. Link, A. Furube, M. B. Mohamed, T. Asahi, H. Masuhara, and M. A. El-Sayed, J. Phys. Chem. B **106** (2002).
[110] C. Voisin, D. Christofilos, N. D. Fatti, F. Vallée, B. Prével, E. Cottancin, J. Lermé, M. Pellarin, and M. Broyer, Phys. Rev. Lett. **85**, 2200 (2000).
[111] S. Park, M. Pelton, M. Liu, P. Guyot-Sionnest, and N. F. Scherer, J. Phys. Chem. C **111**, 116 (2007).
[112] A. A. Maznev, K. A. Nelson, and J. A. Rogers, Opt. Lett. **23**, 1319 (1998).
[113] T. Itoh, T. Asahi, and H. Masuhara, Appl. Phys. Lett. **79**, 1667 (2001).
[114] K. Imura, T. Nagahara, and H. Okamoto, J. Phys. Chem. B **108**, 16344 (2004).
[115] M. Pelton, M. Liu, S. Park, N. F. Scherer, and P. Guyot-Sionnest, Phys. Rev. B **73**, 155419 (2006).
[116] Y. Matsuo and K. Sasaki, Jpn. J. Appl. Phys. **40**, 6143 (2001).

© 2008 by WILEY-VCH Verlag GmbH & Co. KGaA, Weinheim

[117] O. L. Muskens, N. D. Fatti, and F. Vallée, Nano Lett. **6**, 552 (2006).
[118] M. A. van Dijk, M. Lippitz, and M. Orrit, Phys. Rev. Lett. **95**, 267406 (2005).
[119] M. A. van Dijk, M. Lippitz, D. Stolwijk, and M. Orrit, Opt. Express **15**, 2273 (2007).
[120] A. M. Glass, P. F. Liao, J. G. Bergman, and D. H. Olson, Opt. Lett. **5**, 368 (1980).
[121] D. A. Weitz, S. Garoff, C. D. Hanson, T. J. Gramila, and J. I. Gersten, Opt. Lett. **7**, 89 (1982).
[122] A. Leitner, M. E. Lippitsch, S. Draxler, M. Reigler, and F. R. Aussenegg, Appl. Phys. B **36**, 105 (1985).
[123] O. Kulakovich, N. Stekal, A. Yaroshevich, S. Maskevich, S. Gaponenko, I. Nabiev, U. Woggon, and M. Artemyev, Nano Lett. **2**, 1449 (2002).
[124] V. K. Komarala, Y. P. Rakovich, A. L. Bradley, S. J. Byrne, Y. K. Gun'ko, N. Gaponik, and E. Eychmüller, Appl. Phys. Lett. **89**, 253118 (2006).
[125] K. T. Shimizu, W. K. Woo, B. R. Fisher, H. J. Eisler, and M. G. Bawendi, Phys. Rev. Lett. **89**, 117401 (2002).
[126] K. Ray, R. Badugu, and J. R. Lakowicz, J. Am. Chem. Soc. **128**, 8993 (2006).
[127] Y. Ito, K. Matsuda, and Y. Kanemitsu, Phys. Rev. B **75**, 033309 (2007).
[128] E. Dulkeith, A. C. Morteani, T. Niedereichholz, T. A. Klar, J. Feldmann, S. A. Levi, F. C. J. M. van Veggel, D. N. Reinhoudt, M. Möller, and D. I. Gittins, Phys. Rev. Lett. **89**, 203002 (2002).
[129] B. Dubertret, M. Calame, and A. J. Libchaber, Nature Biotech. **19**, 365 (2001).
[130] D. J. Maxwell, J. R. Taylor, and S. Nie, J. Am. Chem. Soc. **124**, 9606 (2002).
[131] C. S. Yun, A. Javier, T. Jennings, M. Fisher, S. Hira, S. Peterson, B. Hopkins, N. O. Reich, and G. F. Strouse, J. Am. Chem. Soc. **127**, 3115 (2005).
[132] E. Dulkeith, M. Ringler, T. A. Klar, J. Feldmann, A. M. Javier, and W. J. Parak, Nano Lett. **5**, 585 (2005).
[133] O. G. Tovmachenko, C. Graf, D. J. van den Heuvel, A. van Blaaderen, and H. C. Gerritsen, Adv. Mater. **18**, 91 (2006).
[134] N. Liu, B. S. Prall, and V. I. Klimov, J. Am. Chem. Soc. **128**, 15362 (2006).
[135] G. Schneider, G. Decher, N. Nerambourg, R. Praho, M. H. V. Werts, and M. Blanchard-Desce, Nano Lett. **6**, 530 (2006).
[136] T. Pons, I. L. Medintz, K. E. Sapsford, S. Higashiya, A. F. Grimes, D. S. English, and H. Mattoussi, Nano Lett. **7**, 3157 (2007).
[137] J. Lee, A. O. Govorov, J. Dulka, and N. A. Kotov, Nano Lett. **4**, 2323 (2004).
[138] J. Lee, T. Javed, T. Skeini, A. O. Govorov, G. W. Bryant, and N. A. Kotov, Angew. Chem. Int. Ed. **45**, 4819 (2006).
[139] Y. Chen, K. Munechika, and D. S. Ginger, Nano Lett. **7**, 690 (2007).
[140] Z. Gueroui and A. Libchaber, Phys. Rev. Lett. **93**, 166108 (2004).
[141] S. Kühn, U. Håkanson, L. Rogobete, and V. Sangoghdar, Phys. Rev. Lett. **97**, 017402 (2006).
[142] P. Anger, P. Bharadwaj, and L. Novotny, Phys. Rev. Lett. **96**, 113002 (2006).
[143] G. Mie, Ann. Phys. (Leipzig) **330**, 377 (1908).
[144] R. Gans, Ann. Phys. **342**, 881 (1912).
[145] T. L. Ferrell and P. M. Echenique, Phys. Rev. Lett. **55**, 1526 (1985).
[146] T. Atay, J. H. Song, and A. V. Nurmikko, Nano Lett. **4**, 1627 (2004).
[147] K. L. Kliewer and R. Fuchs, Phys. Rev. **153**, 498 (1967).
[148] J. Ashley and L. Emerson, Surf. Sci. **41**, 615 (1974).
[149] C. A. Pfeiffer, E. N. Economou, and K. L. Ngai, Phys. Rev. B **10**, 3038 (1974).
[150] R. Fuchs, Phys. Rev. B **11**, 1732 (1975).
[151] L. Davis, Phys. Rev. B **14**, 5523 (1976).
[152] J. Aizpurua, A. Rivacoba, and S. P. Apell, Phys. Rev. B **54**, 2901 (1996).
[153] R. Rupin, Phys. Rev. B **26**, 3440 (1982).
[154] F. Claro, Phys. Rev. B **25**, 7875 (1982).
[155] F. J. García-Vidal, J. M. Pitarke, and J. B. Pendry, Phys. Rev. Lett. **78**, 4289 (1997).
[156] J. M. Pitarke, F. J. García-Vidal, and J. B. Pendry, Phys. Rev. B **57**, 15261 (1998).
[157] E. K. Miller, J. Electromagn. Waves Appl. **8**, 1125 (1994).
[158] E. M. Purcell and C. R. Pennypacker, Astrophys. J. **186**, 705 (1973).
[159] B. T. Draine and P. J. Flatau, J. Opt. Soc. Am. A **11**, 1491 (1994).
[160] O. J. F. Martin, C. Girard, and A. Dereux, Phys. Rev. Lett. **74**, 526 (1995).
[161] C. H. Hafner and R. Ballist, Int. J. Comp. Elect. Elect. Eng. **2**, 1 (1983).
[162] J. B. Pendry and A. MacKinnon, Phys. Rev. Lett. **69**, 2772 (1992).
[163] K. M. Leung and Y. F. Liu, Phys. Rev. B **41**, 10188 (1990).
[164] F. J. García de Abajo and A. Howie, Phys. Rev. Lett. **80**, 5180 (1998).
[165] J. Aizpurua, G. W. Bryant, L. J. Richter, F. J. García de Abajo, B. K. Kelly, and T. Mallouk, Phys. Rev. B **71**, 235420 (2005).
[166] S. Link, M. B. Mohamed, and M. A. El-Sayed, J. Phys. Chem. B **103**, 3073 (1999).
[167] S. Eustis and M. A. El-Sayed, J. Phys. Chem. B **109**, 16350 (2005).
[168] S. Eustis and M. A. El-Sayed, J. Appl. Phys. **100**, 44324 (2006).
[169] K. Lee and M. A. El-Sayed, J. Phys. Chem. B **109**, 20331 (2005).
[170] P. K. Jain, K. S. Lee, I. H. El-Sayed, and M. A. El-Sayed, J. Phys. Chem. B **110**, 7238 (2006).
[171] K. S. Lee and M. A. El-Sayed, J. Phys. Chem. B **110**, 19220 (2006).
[172] E. Hao and G. C. Schatz, J. Chem. Phys. **120**, 357 (2004).
[173] E. K. Payne, K. L. Shuford, S. Park, G. C. Schatz, and C. A. Mirkin, J. Phys. Chem. B **110**, 2150 (2006).
[174] A. Brioude, X. C. Jiang, and M. P. Pileni, J. Phys. Chem. B **109**, 13138 (2005).
[175] S. E. Sburlan, L. A. Blanco, and M. Nieto-Vesperinas, Phys. Rev. B **73**, 035403 (2006).
[176] S. W. Prescott and P. J. Mulvaney, J. Appl. Phys. **99**, 123504 (2006).
[177] C. Noguez, J. Phys. Chem. C **111**, 3806 (2007).
[178] B. N. Khlebtsov and N. G. Khlebtsov, J. Phys. Chem. C **111**, 11516 (2007).
[179] G. W. Bryant, F. J. García de Abajo, and J. Aizpurua, Nano Letters **8**, 631 (2008).

© 2008 by WILEY-VCH Verlag GmbH & Co. KGaA, Weinheim

[180] P. Mühlschlegel, H. J. Eisler, O. J. F. Martin, B. Hecht, and D. W. Pohl, Science **308**, 1607 (2005).
[181] E. Cubukcu, E. A. Kort, K. B. Crozier, and F. Capasso, Appl. Phys. Lett. **89**, 093120 (2006).
[182] L. Novotny, Phys. Rev. Lett. **98**, 266802 (2007).
[183] O. L. Muskens, V. Giannini, J. A. Sánchez-Gil, and J. G. Rivas, Nano Lett. **7**, 2871 (2007).
[184] F. Hao, C. L. Nehl, J. H. Hafner, and P. Nordlander, Nano Lett. **7**, 729 (2007).
[185] J. Aizpurua, G. Hoffmann, S. P. Apell, and R. Berndt, Phys. Rev. Lett. **89**, 156803 (2002).
[186] M. Ringler, T. A. Klar, A. Schwemer, A. S. Susha, J. Stehr, G. Raschke, S. Funk, M. Borowski, A. Nichtl, K. Kürzinger, R. T. Phillips, and J. Feldmann, Nano Lett. **7**, 2753 (2007).
[187] E. Prodan, C. Radloff, N. J. Halas, and P. Nordlander, Science **302**, 419 (2003).
[188] P. Nordlander, C. Oubre, E. Prodan, K. Li, and M. I. Stockman, Nano Lett. **4**, 899 (2004).
[189] I. Romero, J. Aizpurua, G. W. Bryant, and F. J. García de Abajo, Opt. Express **14**, 9988 (2006).
[190] R. Fuchs and F. Claro, Phys. Rev. B **35**, 3722 (1987).
[191] E. Prodan, P. Nordlander, and N. J. Halas, Nano Lett. **3**, 1411 (2003).
[192] A. Castro, M. A. L. Marques, J. A. Alonso, and A. Rubio, J. Comp. Theoret. Nanoscience **1**, 230 (2004).

Wiley-VCH BOOK SHOP

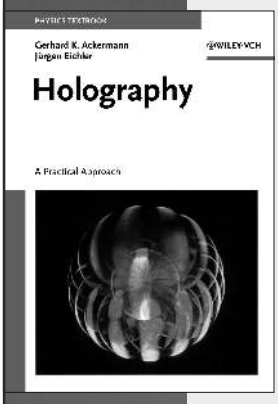

G. K. Ackermann / J. Eichler
Holography
A Practical Approach
From the fundamentals to advanced experiments, this proven textbook guides students using a practical approach backed by real-world materials. Contains exercises plus solutions as well as instructions for over 20 experiments.
337 pp, pr, € 69.00
ISBN: 978-3-527-40663-0

R. B. Wehrspohn / H.-S. Kitzerow / K. Busch (eds.)
Nanophotonic Materials
Photonic Crystals, Plasmonics, and Metamaterials
Photonic Crystals, plasmonic materials and metamaterials are currently hot topics in photonics research. The current book gives an overview of these novel materials, spanning the entire range from fundamentals to applications and illustrated throughout in full colour.
approx. 447 pp, cl, € 159.00
ISBN: 978-3-527-40858-0

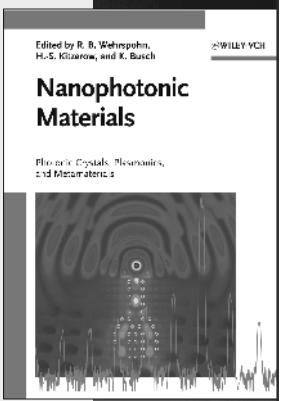

Prices are subject to change without notice.

You can order online via **http://www.wiley-vch.de**
Wiley-VCH Verlag GmbH & Co. KGaA · POB 10 11 61 · D-69451 Weinheim, Germany
Phone: 49 (0) 6201/606-400 · **Fax:** 49 (0) 6201/606-184 · **E-Mail:** service@wiley-vch.de

WILEY-VCH

© 2008 by WILEY-VCH Verlag GmbH & Co. KGaA, Weinheim